2008

A capacity-approaching coded modulation scheme for non-coherent fading channels

Youngjeon Cho
Louisiana State University and Agricultural and Mechanical College

A CAPACITY-APPROACHING CODED MODULATION SCHEME FOR NON-COHERENT FADING CHANNELS

A Thesis

Submitted to the Graduate Faculty of the
Louisiana State University and
Agricultural and Mechanical College
in partial fulfillment of the
requirements for the degree of
Master of Science in Electrical Engineering

In

The Department of Electrical and Computer Engineering

By
Youngjeon Cho
Bachelor of Engineering, Korea Military Academy, 1999
May 2008

Acknowledgments

It is a pleasure to thank the many people who made this thesis possible. First and foremost, I would like to thank Professor Xue-Bin Liang for his supervision, mentorship, moral and technical support during my graduate research studies at Louisiana State University. I truly appreciate his guidance and wisdom in executing this study. I also thank Professor Guoxiang Gu and Professor Shuangqing Wei for their invaluable help and willingness to serve on my dissertation research committee.

My wife, Eunhye, and my daughter, Solji, gave me encouragement and delight. I really could not have done this without them. Finally, I would like to thank the Korean Army for sending me here to learn many things.

Table of Contents

List of Figures

Abstract

Approaching the Shannon limit of the communication channels has been studied by many researchers to efficiently and reliably transmit data through the channels. To solve this problem, various methods and schemes have been proposed for approaching the theoretical limit for Shannon's channel capacity. Among them, both low-density parity check (LDPC) codes and Turbo codes have been proposed to minimize the bit error rate (BER). Therefore, understanding of LDPC codes and Turbo codes is useful for their applications in modern communication systems.

The study about non-coherent channels, which do not require explicit knowledge or estimation of the channel state information, has become a major issue in mobile communication. Specifically, a new signaling scheme called unitary space-time modulation has been invented which is suitable for non-coherent channels. Combining channel coding with unitary space-time modulation is expected to make good performance for non-coherent fading channels.

In this thesis, non-coherent capacity of a mobile communication channel in Rayleigh flat fading is calculated for the case of coherence time of length two. Also, LDPC codes and Turbo codes are combined with unitary space-time modulation to enhance the efficiency and reliability of communication over non-coherent fading channels. The performance results are compared to the calculated channel capacity. Simulation results show that both LDPC codes and Turbo codes are well performed for non-coherent fading channels. The LDPC and Turbo coded unitary space-time modulation schemes have BER performance much better than the uncoded modulation schemes and the performance is close to the calculated channel capacity.

Chapter 1 Introduction

The role of communication has been changed. People are no longer satisfied with voice communication. They want to watch TV and to connect to the internet with their cell phones. In order to satisfy people's desires, the technology in wireless communication has been developed rapidly and new terminology has been emerged in this field. Remarkable breakthrough has been made in channel coding area to minimize bit error rate (BER) which are turbo codes and low-density parity check (LDPC) codes.

However, fading may be too fast to get the knowledge of the channel state information at the receiver. So, the case where the channel state information is unknown to the transmitter and the receiver has been studied. In this chapter, the basic background of a mobile communication system will be presented.

1.1 Channel Coding

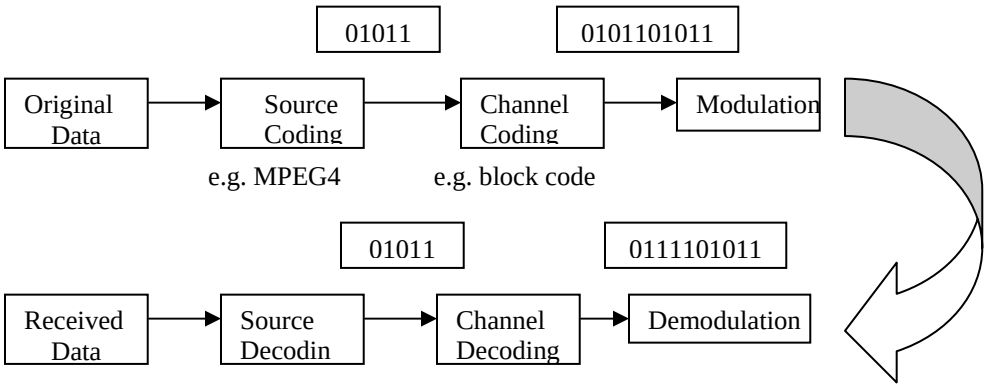

Figure 1.1 Channel coding at transmitter and receiver.

In modern society, it is very important to get reliability of data. However, as the quantity of data increased, it has high possibility to produce errors. So, error-correcting coding emerged and has been developed to minimize the errors. The principle for error detection and correction is simple. Figure 1.1 shows the basic diagram of communication

and illustrates how channel coding changes bits. Channel encoder receives data 1 or 0, but it adds redundant data and sends it to the modulator. For example, if there is an information bit, '1', which will be sent to the receiver, channel encoder adds redundancy and produces 111. Then, the coded data go to the modulator. Receiver can detect '1' as long as error occurs just one time like 101 or 110. Thus, we can assume that error detection/correction adds redundancy to the original data so that receiver can detect the information error.

Channel coding is an error-correcting coding by which codes can be constructed to detect and correct errors which may be caused by noise and interference. A mobile communication system would be unreliable without channel coding. The modern approach to error control in digital communications originated from the work of Shannon [8] and Hamming [9]. Since then, many different error correcting codes have emerged. Historically, these codes have been included block codes and convolutional codes. The main difference for the two codes is the presence of memory in the encoders. Various approaches have been proposed for approaching the theoretical limit for Shannon's channel capacity. The well-known channel coding schemes to approach Shannon's limit have LDPC codes and Turbo codes among others.

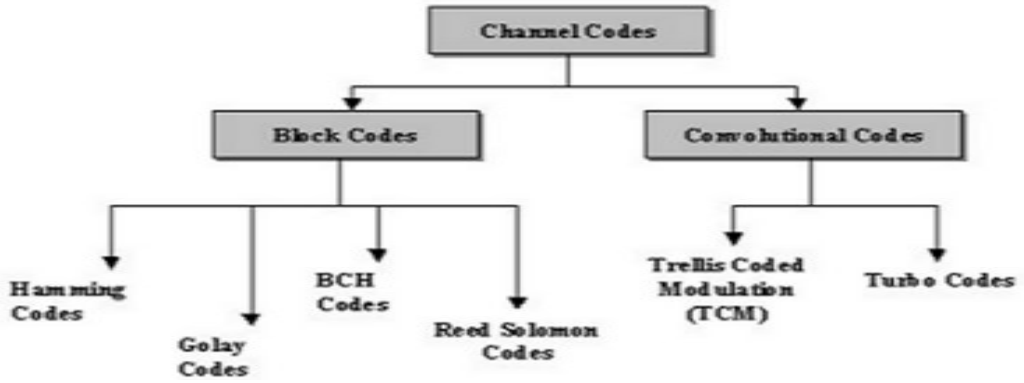

Figure 1.2 Types of channel codes (Adopted from Ref. [32])

Figure 1.2 illustrates types of channel codes. It also shows that Turbo codes use convolutional codes and iterative decoding. Likewise, LDPC codes also use iterative decoding to approach Shannon limit, but LDPC codes is block codes. Sum-product algorithm which is used in LDPC codes has low complexity as compared to the maximum posteriori probability (MAP) algorithm in Turbo codes. Richardson's research shows that LDPC codes can approach the Shannon limit closer than Turbo codes with the block length 10^6 and code rate $\frac{1}{2}$ [21]. Both LDPC codes and Turbo codes are main streams in error-correction channel coding for digital communication system.

1.2 Small Scale Fading

Fading is the channel condition varying as time or frequency. It is caused by many reasons such as time variation of received signal, changes in transmission paths, and movement of antenna. Small scale fading plays important role in a mobile communication and is dominated by two factors, multi path propagation and Doppler shift. Figure 1.3 illustrates multi paths in mobile communication.

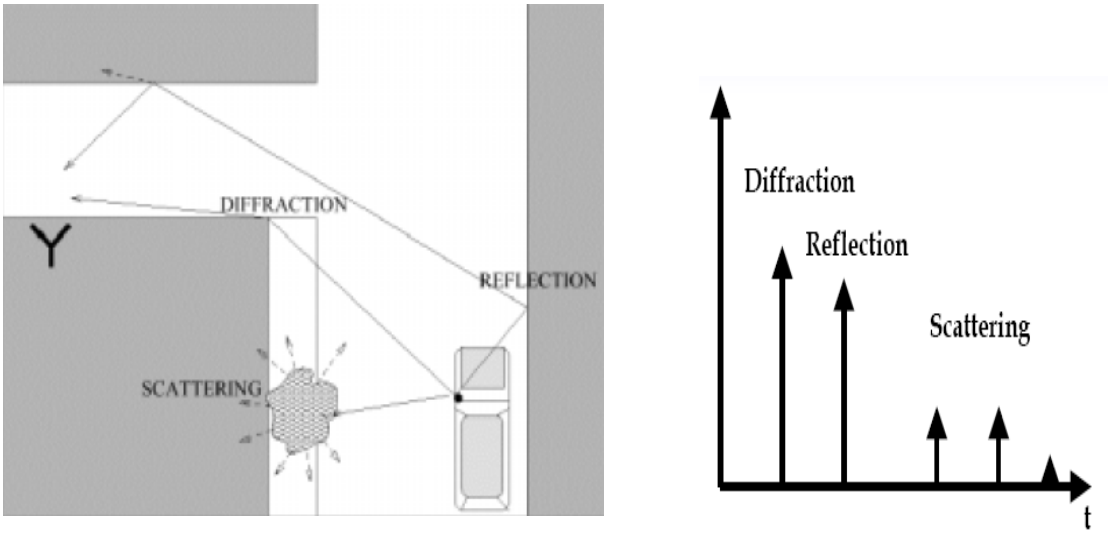

Figure 1.3 Many paths in a mobile communication (diffraction, reflection, scattering) (Adopted from Ref. [31])

Signals can take many different paths between transmitter and receiver due to reflection, scattering, diffraction. If line of sight (LOS) exists, LOS plays major important role in communication. However, it is very difficult to get LOS in mobile communication. We need to consider the environment where LOS does not exist. In this case, diffraction and reflection can be primary factors at the receiver. The multi path propagation makes signals arrive at the receiver at different times. It is called delay spread. In mobile communication, delay spread is even worse if transmitter and receiver move and channel characteristics change over time and location. When multipath components of one pulse overlap components of subsequent pulse, it is called intersymbol interference (ISI).

1.2.1 Frequency Flat Fading

The wireless channel is said to be flat fading, when the channel has constant gain and linear phase and linear response is much larger than the bandwidth of the signal [2]. Let B_S be the bandwidth of the signal and B_c be the coherence bandwidth, then for flat fading channel, $B_c >> B_S$. It means that when coherence bandwidth is larger than bandwidth of the signal, flat fading channel happens. This yields another important fact that ISI is negligible in flat fading channel [4]. Figure 1.4 illustrates how to divide wireless channel into two types of fading channels.

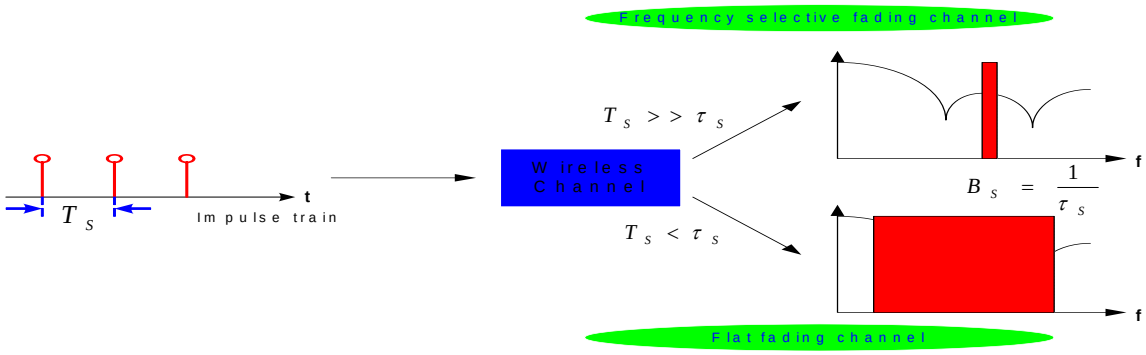

Figure 1.4 Two types of wireless channel (Adopted from Ref. [31])

1.3 Unitary Space-Time Modulation

A non-coherent communication system is a system where channel state information is not known at the receiver end, i.e., fading coefficients are not known at the receiver. Unitary space-time modulation is invented for multiple antennas in non-coherent channel that operates in a Rayleigh flat-fading environment [10]. It is a signaling scheme which constellation comprising complex-valued signals $\Phi_l, l = 1, \cdots, L$ with respect to time among the transmitter antennas. Space-time signals Φ_l are T × M matrix where M is the number of transmits antennas and T is the coherence time during which the fading is approximately constant. Figure 1.5 shows when three transmitter and three receiver antennas are used.

However, we only consider a mobile communication system that employs one transmitter antenna and one receiver antenna that operates in a Rayleigh flat fading environment. The model at the receiver can be described as follows.

$$X = \sqrt{\rho} SH + W \qquad (1\text{-}1)$$

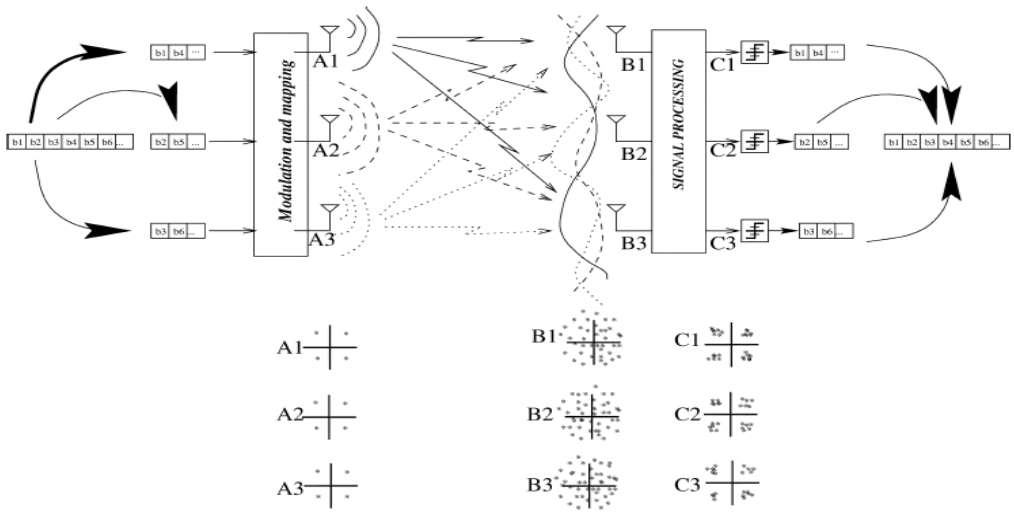

Figure 1.5 Basic spatial multiplexing scheme with three Tx and three Rx antennas. Ai, Bi, and Ci represent symbol constellations (Adopted from Ref. [11])

where X is the T×1 received signal, ρ is the signal to noise ratio(SNR) at the receiver antenna, S is the T×1 transmit signal, H is the complex-valued fading coefficient which is constant for t = 1,…,T, and W is the T×1 additive white Gaussian noise (AWGN)

Fading coefficient H is constant for T symbol period (In this thesis, T = 2 will be only considered). Fading coefficient H and Gaussian noise W are independent and identically distributed $CN(0,1)$. The transmitted signal power can be written as

$$E|s_t|^2 = 1, \qquad t = 1,\ldots,T \tag{1-2}$$

If coherence interval T is changed, transmit signal *s* should be also changed using the equation of (1-2) in order to get equal transmitted power.

A constellation of L unitary space-time signals, $\{S_1,\ldots S_L\}$ are defined to comprise of T ×M complex-valued matrices such that $S_l = \sqrt{T}\phi_l$, l=1,…,L, where Φ_l is an isotropically distributed T × M matrix with the constraints $\phi_1^H\phi_1 = \ldots = \phi_L^H\phi_L = I_M$ [10]. The columns of Φ_l are orthonormal. Because of the maximum-likelihood (ML) algorithm for a constellation of unitary space-time signals, which is shown in [5], we seek to the singular values of $\phi_2^H\phi_1$ as small as possible to minimize pair wise probability error.

1.4 Problem Statement

Combining LDPC codes or turbo codes with non-coherent fading channels has been performed by some researchers [9][15][27]. The results of those papers show that coded modulation schemes outperform uncoded modulation. However, those papers did not use optimum codewords for unitary space-time modulation. Moreover, they did not compute the capacity for comparing the BER performance with the capacity of the non-coherent channels. One contribution of this thesis is to calculate capacity for certain cases based on

Hassibi's paper [7]. With the calculated capacity, either LDPC codes or Turbo codes will be combined with unitary space time modulation to see if the results can approach the Shannon limit. In order to get the best results, optimum codewords will be used for certain coherent time T.

1.5 Thesis Organization

The rest of this thesis is organized as follows. Chapter 2 presents the capacity for the non-coherent fading channel in the case of coherence time T =2. Chapter 3 gives a brief review of Turbo codes and Chapter 4 presents LDPC codes. In Chapters 3 and 4, we will see the simulation results for LDPC and Turbo codes over AWGN channels. Chapter 5 introduces the channel model which is used for simulation of LDPC and Turbo coded modulation schemes for non-coherent fading channels. Chapter 6 presents the simulation results. The conclusion of the thesis is given in Chapter 7.

Chapter 2 Capacity for Non-Coherent Fading Channels

We want to compute capacity for mobile communication with no channel state information available either to the transmitter or to the receiver. Hassabi and Marzetta computed the capacity using isotropically random unitary inputs [7], but the paper only introduced results for mutual information per symbol versus duration of coherence interval T. Since our goal of this thesis is to compare the capacity with coded performance, detailed capacity for certain cases are needed. In this chapter, We will briefly describe how to obtain the close form capacity which was introduced in [7]. Then, the result will be applied to the special case which one transmit and one receive antenna are used with T=2.

2.1 Signal Model

The propagation coefficients are assumed to be constant for T symbol periods. If M transmit and N receive antennas are given, the signal model can be given by

$$X=\sqrt{\rho / M}\,SH + W \qquad (2\text{-}1)$$

where ρ is the signal to noise ratio (SNR)

The signal S is the product of two independent random matrices [1] and can be written by

$$S=\sqrt{T}\,\Phi D \qquad (2\text{-}2)$$

where Φ is a unitary matrix, and D is a nonnegative real diagonal matrix.

In this thesis, D= I_M will be considered in the paper [7].

2.2 Mutual Information

The mutual information is given by

$$I(X;S)= E\left[\log \frac{P(X|S)}{P(X)}\right] = E\left[\log P(X|S) - \log P(X)\right] \qquad (2\text{-}3)$$

where X is the received signals and S is the transmit signals.

Equation of (2-2) shows that the mutual information I(X;S) can be obtained provided that $\log P(X|S)$, and $\log P(X)$ are calculated. To get these probabilities, Marzetta's paper [5] is referred which offered properties of capacity for non-coherent fading channel. The conditional probability density of the received signals for non-coherent channel is

$$p(X|S) = \frac{\exp(-tr\{\Lambda^{-1} X X^{+}\})}{\pi^{TN} \det^{N} \Lambda} \tag{2-4}$$

where $\Lambda = \mathrm{I_T} + (\rho / M) S\ S^{H}$ is covariance matrix of the columns of X.

From the equation of (2-1), we can rewrite the equation of (2-4) as

$$p(X|S) = \frac{\exp[-trX^{+}(\mathrm{I_T} + \rho\beta\Phi D^{2}\Phi^{+})^{-1} X]}{\pi^{TN} \det(\mathrm{I_T} + \rho\beta\Phi D^{2}\Phi^{+})^{N}}$$

$$= \frac{\exp[-trX^{+}X]}{\pi^{TN} \det(\mathrm{I_M} + \rho\beta D^{2})^{N}} \exp\left[tr(X^{+}\Phi(\mathrm{I_M} + \frac{1}{\rho\beta} D^{-2})^{-1}\Phi^{+} X \right] \tag{2-5}$$

where we define $\beta = T / M$.

Also, we can get p(X) from $P(X|D)$, the detailed steps are suggested in [7]. p(X) is written as

$$p(X) = \frac{(-1)^{(T-M)(T-M-1)/2}}{\pi^{TN}} \cdot \frac{\exp(-tr(1-\alpha)X^{+}X)}{(1+\rho\beta)^{MN}} \cdot \frac{\Gamma(T)\cdots\Gamma(M+1)}{\Gamma(T-M)\cdots\Gamma(1)} \det G \tag{2-6}$$

where G is a (T-M) × (T-M) Hankel matrix, $\alpha = \frac{\rho\beta}{1+\rho\beta}$, and G is given by

$$\mathrm{G_{mn}} = \frac{\exp(-\alpha\sigma_k)}{(-\alpha\sigma_k)^{\mathrm{Q}} \prod_{l\neq k} (-\alpha\sigma_k + \alpha\sigma_l)} \left[(1 - \exp(-\alpha\sigma_k)) \cdot \sum_{\mathrm{q}=0}^{\mathrm{Q-1}} \frac{(-\alpha\sigma_k)^{\mathrm{q}}}{\mathrm{q!}} \right], \text{ when Q>0}$$

where σ_k is nonzero eigenvalue of XX^{+}.

Monte Carlo estimate can be used to get mutual information

$$\hat{\mathrm{I}}(\mathrm{X};\mathrm{S}) = \frac{1}{\mathrm{L}}\sum_{l=1}^{\mathrm{L}} \log \frac{p(\mathrm{X}_l \mid \Phi_0)}{p(\mathrm{X}_l)}$$

$$= \frac{1}{\mathrm{L}}\sum_{l=1}^{\mathrm{L}} \log\left(\frac{\Gamma(\mathrm{T}-\mathrm{M})\cdots\Gamma(1)}{\Gamma(\mathrm{T})\cdots\Gamma(\mathrm{M}+1)} \bullet \frac{\exp\left(\alpha \mathrm{tr}\mathrm{X}_l \mathrm{X}_l^{+}\left(-\mathrm{I}_{\mathrm{T}} + \Phi_0\Phi_0^{+}\right)\right)}{(-1)^{(\mathrm{T}-\mathrm{M})(\mathrm{T}-\mathrm{M}-1)/2}\det \mathrm{G}_l} \right) \qquad (2\text{-}7)$$

where $\mathrm{G}_{\mathrm{l}} = \frac{\exp(-\alpha\sigma_k)}{(-\alpha\sigma_k)^{\mathrm{Q}}\prod_{l\neq k}(-\alpha\sigma_k + \alpha\sigma_l)}\left[(1-\exp(-\alpha\sigma_k))\cdot\sum_{\mathrm{q}=0}^{\mathrm{Q}-1}\frac{(-\alpha\sigma_k)^{\mathrm{q}}}{\mathrm{q}!}\right]$.

Equation of (2-7) is the closed form capacity for non-coherent channels which is shown in [7]. However, the closed form involves many matrixes to compute the capacity when T is larger, due to the (T-M) × (T-M) G matrix. In this thesis, we only consider special case for capacity for non-coherent channels with a single transmit and receive antenna for coherence interval T of 2. In order to get the results for this case, we need to do further steps.

2.3 Ultimate Formula

2.3.1 Obtaining G

Because coherence time T is 2 and one transmit and one receive antenna are considered, we can get K= min (T, N) =1, Q = 1, $\Phi_0 = \begin{bmatrix} \mathrm{I}_{\mathrm{M}} \\ 0 \end{bmatrix} = \begin{bmatrix} 1 \\ 0 \end{bmatrix}$.

Therefore Hankel matrix G is written as

$$\mathrm{G}_l = \frac{\exp(-\alpha\sigma_k)}{(-\alpha\sigma_k)^{\mathrm{Q}}\prod_{l\neq k}(-\alpha\sigma_k + \alpha\sigma_l)}\left[(1-\exp(-\alpha\sigma_k))\cdot\sum_{\mathrm{q}=0}^{\mathrm{Q}-1}\frac{(-\alpha\sigma_k)^{\mathrm{q}}}{\mathrm{q}!}\right]$$

$$= \frac{1-\exp(-\alpha\sigma_k)}{-\alpha\sigma_k} \qquad (2\text{-}8)$$

Now, we want to compute σ_k which is nonzero eigenvalue of XX^+.

Let $\mathrm{X}_l = \begin{bmatrix} a_l \\ b_l \end{bmatrix} = \begin{bmatrix} a_0 + a_1 i \\ b_0 + b_1 i \end{bmatrix}$, where a_l, b_l are complex numbers. $\mathrm{X}_l\mathrm{X}_l^+$ can be written

as $\mathrm{X}_l\mathrm{X}_l^+ = \begin{bmatrix} a_l \\ b_l \end{bmatrix}\begin{bmatrix} a_l & b_l \end{bmatrix} = \begin{bmatrix} |a_l|^2 & a_l b_l^* \\ a_l^* b_l & |b_l|^2 \end{bmatrix}$.

Thus, we can get the nonzero eigenvalue of XX^+ is $\sigma_k = |a_l|^2 + |b_l|^2$.

2.3.2 Capacity

Our ultimate goal is to simplify the equation of (2-7). The gamma function, which is shown in equation of (2-7), defines $\Gamma(x)$ =(x-1)!, if x is positive. Since coherence time T is 2 and the number of transmit antenna is 1, the gamma function of (2-7) is calculated by $\frac{\Gamma(\mathrm{T}-\mathrm{M})\cdots\Gamma(1)}{\Gamma(\mathrm{T})\cdots\Gamma(\mathrm{M}+1)} = \frac{\Gamma(1)}{\Gamma(2)} = \frac{0!}{1!} = 1$. We also have $\mathrm{Tr}(\mathrm{X}_l\mathrm{X}_l^+) = |a_l|^2 + |b_l|^2$.

Using these results, the exponential part of $\hat{\mathrm{I}}(\mathrm{X};\mathrm{S})$ can be simplified by

$$\exp\left(\alpha \mathrm{tr}\mathrm{X}_l\mathrm{X}_l^+\left(-\mathrm{I}_\mathrm{T} + \Phi_0\Phi_0^+\right)\right) = \exp\left(\alpha \mathrm{tr}\begin{bmatrix} |a_l|^2 & a_l b_l^* \\ a_l^* b_l & |b_l|^2 \end{bmatrix}\begin{bmatrix} 0 & 0 \\ 0 & -1 \end{bmatrix}\right) = \exp\left(-\alpha |b_l|^2\right)$$

Thus, we can get the capacity

$$\hat{\mathrm{I}}(\mathrm{X};\mathrm{S}) = \frac{1}{\mathrm{L}}\sum_{l=1}^{\mathrm{L}} \log\frac{\exp(-\alpha|b_l|^2)}{\det \mathrm{G}_l} = \frac{-\alpha}{\mathrm{L}}\sum_{l=1}^{\mathrm{L}}|b_l|^2 - \frac{1}{\mathrm{L}}\sum_{l=1}^{\mathrm{L}}\log\frac{1-\exp(-\alpha\sigma_k)}{\alpha\sigma_k} \qquad (2\text{-}9)$$

2.4 Simulation Result

To simulate the equation of (2-9), a and b should be determined. Since a and b are distributed according to the equation of (2-4), the conditional probability of X is written as

$$p(X|S)=\frac{\exp\left[-tr\begin{bmatrix}a^2 & 0\\ 0 & b^2\end{bmatrix}\right]}{\pi^2(1+\rho\beta)}\exp\left[tr\begin{bmatrix}a & b\end{bmatrix}\begin{bmatrix}1\\0\end{bmatrix}\left[1+\frac{1}{\rho\beta}\right]^{-1}\begin{bmatrix}1 & 0\end{bmatrix}\begin{bmatrix}a\\b\end{bmatrix}\right]$$

$$=\frac{1}{\pi^2}\frac{1}{1+2\rho}\exp\left[-\frac{1}{1+2\rho}a_0^2-\frac{1}{1+2\rho}a_1^2-b_0^2-b_1^2\right] \qquad (2\text{-}10)$$

With equations of (2-9) and (2-10), the graph of capacity for non coherent fading channel is obtained. Matlab is used to make this simulation.

Figure 2.1 illustrates the capacity for the case of T = 2. L=30000 is used for Monte Carlo estimate. The graph shows that when the SNR is increased, capacity can also be increased. The results will be used in Chapter 6, where LDPC codes and Turbo codes are depicted and they will be compared to this capacity. The graph only considered coherence time T of 2. The graph for different Ts can be obtained by the same idea that

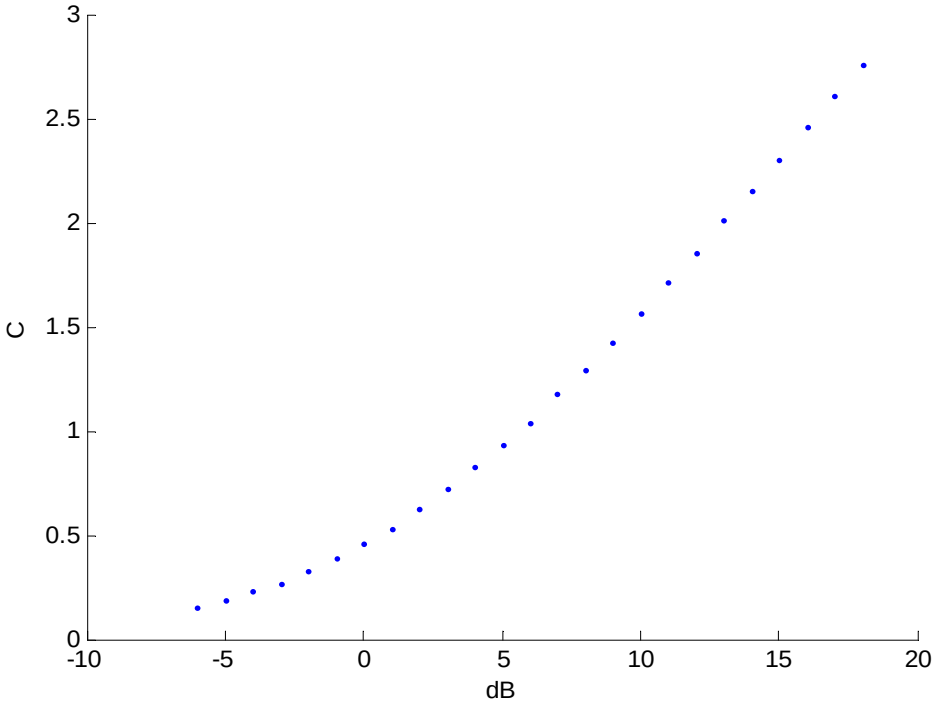

Figure 2.1 Capacity versus SNR, single antenna used and only considered T = 2.

we proceeded in this Chapter. However, it is not surprising that increasing T causes more complexity to calculate capacity.

Chapter 3 Turbo Codes

Turbo codes, which was proposed in1993 by C. Berrou et al [13], achieves almost reliable data communication at signal-to-noise ratio that is very close to the Shannon-limit despite of its complexity. Since turbo encoder consists of two constituent convolutional codes separated by an interleaver, linear convolutional codes will be briefly explained to understand Turbo codes in this Chapter. Also, the MAP algorithm, which is used at the turbo decoder, will be discussed.

3.1 Convolutional Codes

Convolutional codes generate coded symbols by passing the information bits through a linear finite-state shift register with tap [3]. Figure 3.1 shows two types of convolutional codes in which one is recursive and the other is non-recursive. Tapped outputs of shift register are added by modulo-2 addition and the outputs of modulo-2 adders are multiplexing.

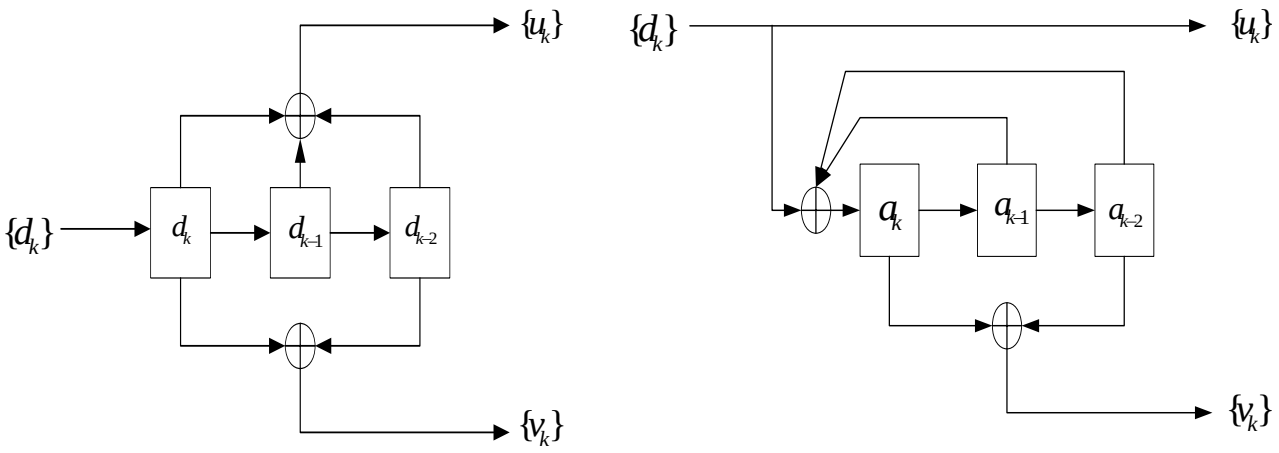

(a) Non-recursive systematic (b) Recursive systematic

Figure 3.1 Two types of convolutional codes.

Let *n* be the number of output bits, *k* be the number of input bits and *m* be the number of memory registers. The quantity *k/n* is called the code rate. The constraint length L represents the number of bits in the encoder memory that affects the generation of the *n* output bits. It is defined as L = *k (m*-1*).* Current output at the encoder depends on the current input and *m* previous inputs of the encoder.

Encoder generator is used to make convolution encoder. Assuming that Y_k is the output bits of the encoder, convolutional encoder can be written as

$$Y_k = \sum_{i=0}^{L-1} g_i d_{k-i} \text{ mod. } 2 \qquad (3\text{-}1)$$

where G : { g_i } is the encoder generator which is one or zero. It can be represented in octal form.

Graphically, there are three ways in which we can look at the encoder or decoder to gain better understanding of its operation. These are State Diagram, Tree Diagram, and Trellis Diagram. Figure 3.2 shows trellis diagram which is a powerful way of describing the decoding. In Figure 3.2, 8 different bits combinations (8 states) represent 3 memory registers. There are two outputs for each state. Since memory registers have no previous data before data is encoded, the trellis begins at state 000.

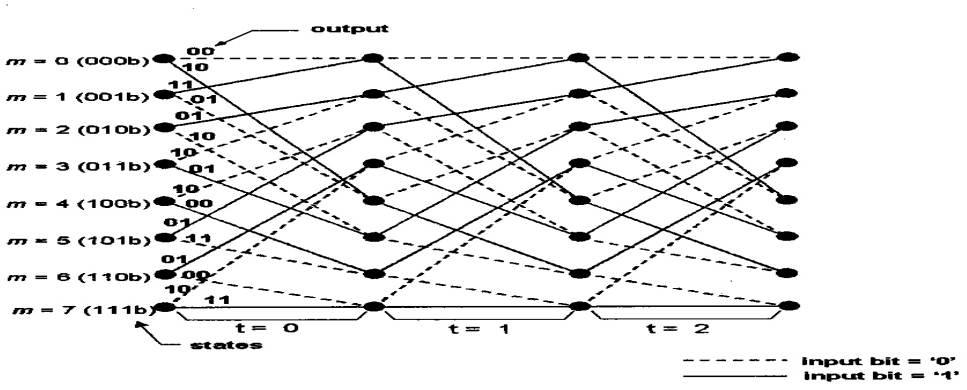

Figure 3.2 Trellis diagram for 8 states. (Adopted from Ref. [16])

3.2 Turbo Encoder

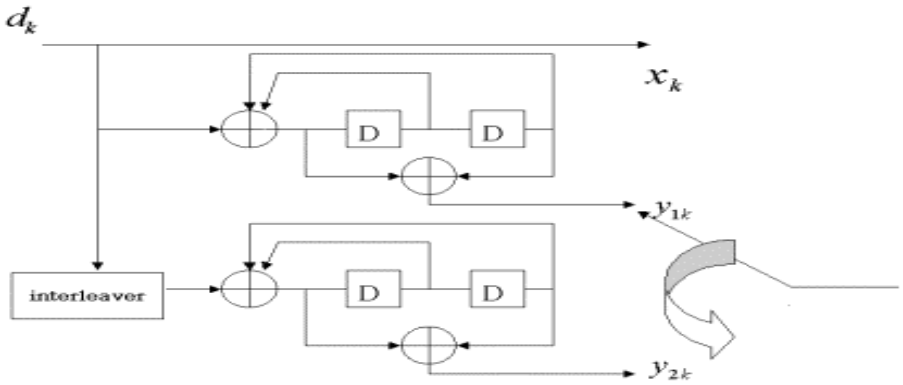

Figure 3.3: Turbo encoder.

The common form of convolutional encoder is the non-recursive systematic convolutional encoder which is shown in Figure 3.3. However, the turbo encoder consists of two recursive systematic convolutional encoders separated by an interleaver.

As turbo encoder is systematic, the message bit d_k produces x_k without processing encoding. The message bit d_k is also encoded by the first encoder to produce parity bits Y_{1k}. And interleaved message bit d_k is encoded by the second encoder to make another parity bits Y_{2k}. Figure 3.3 also shows how to combine two systematic convolutional encoders with one interleaver.

The rate of the Turbo codes can be varied by the symbol size of input and output. If punctured code, which produces codes of many different rates, is used, different code rate can be obtained by deleting output bits according to a chosen puncturing pattern [13].

3.2.1 Interleaver

An interleaver is an device that permutes the ordering of a sequence of symbols from input, i.e., the symbols at the input are ordered by interleaver [28]. This interleaver can eliminate the correlation among bits so that burst errors can be avoided. There are many

kinds of interleavers such as block interleaver, helical interleaver, and random interleaver. Turbo codes uses random interleaver which is well known to the best interleaver. It is hard to find the correlation among input bits, when random interleaver is used. Because the interleaver puts the input bits randomly.

3.3 Turbo Decoder

Maximum a Posteriori (MAP) algorithm was modified to be used for turbo codes in 1993 [13]. MAP algorithm for turbo decoder uses two decoding stages. It is called BCJR algorithm which is named after the inventor's name (Bahl, Cocke, Jelinek, and Raviv). This algorithm minimizes the bit error rate at the turbo decoder. The main flow of BCJR algorithm is that the decoder receives all the bits (noise added) of one frame and computes the probabilities for all paths, and outputs the soft-output.

Two types of parity bits are added noise and faded through channels. And then, each parity bits go to different decoders. Figure 3.4 shows turbo decoder in which two decoders are used. Each of the two decoding stages uses a BCJR algorithm to solve MAP detection problem. In Figure 3.4, Decoder 1 receives information sequence *x* and parity sequence $y^{(1)}$ which is obtained from the first convolutional encoder.

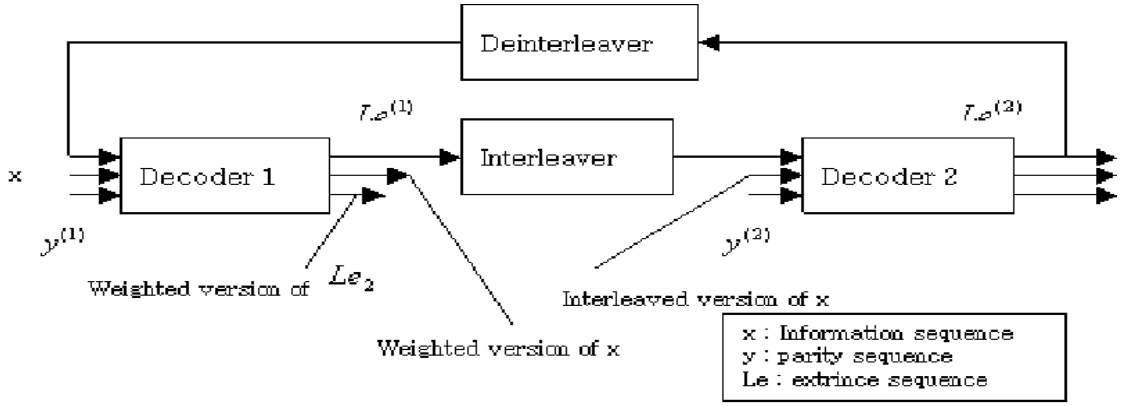

Figure 3.4 Block diagram of turbo decoder.

With x and parity bits $y^{(1)}$, the Decoder 1 produces extrinsic information L_e^1 . The Decoder 2 receives interleaved extrinsic information L_e^1 from Decoder 1. Decoder 2 also receives parity sequence $y^{(2)}$ which is interleaved data from the second convolutional code at the transmitter in order to makes the extrinsic information L_e^2 . Deinterleaver changes interleaved L_e^2 into original bits sequence and this extrinsic information goes back to the Decoder 1. This procedure iterates several times until no errors can be found.

3.3.1 The MAP Decoding Algorithm

At the receiver, log-likelihood can be represented as follows

$$L(d_k) = \log \frac{P_r(d_k = 1 \mid observation)}{P_r(d_k = 0 \mid observation)} \tag{3-2}$$

where $P_r(d_k = i \mid observation)$ is the APP of the data bit. If $L(d_k) \geq 0$, the decoded bit is 1, otherwise, the decoded bit is 0.

Let $\lambda_k(m) = \Pr\left\{S_k = m \middle| R_1^N\right\}$, the APP of a decoded data bit is equal to:

$$P\{d_k = i \mid R_1^N\} = \sum_m \lambda_k^i(m) \qquad \text{i = 0, 1} \tag{3-3}$$

where $R_1^N = \{R_1^{k-1}, R_k, R_{k+1}^{N+1}\}$

Bayes' rule is $P(A \mid B,C,D) = \dfrac{P(A,B,C,D)}{P(B,C,D)} = \dfrac{P(B \mid A,C,D)P(A,C,D)}{P(B,C,D)}$

$$= \frac{P(B \mid A,C,D)P(D \mid A,C)P(A,C)}{P(B,C,D)}$$

Using Bayes' rule, $\lambda_k^i(m)$ can be rewritten by

$$\lambda_k^i(m) = P(R_1^{K-1} \mid d_k = i, S_k = m, R_k^N)P(R_{K+1}^N \mid d_k = i, S_k = m, R_k^N)$$
$$\times P(d_k = i, S_k = m, R_k^N) / P(R_1^N) \tag{3-4}$$

To simplify the equation of (3-4), let us introduce three auxiliary metrics

$\alpha_k(m) = \Pr\{S_k = m, R_1^k\}$, $\beta_k(m) = \Pr\{R_{k+1}^N | S_k = m\}$ and $\gamma_k(m) = \Pr\{S_k = m, R_k | S_{k-1} = m'\}$,

where $\alpha_k(m)$ is a forward state metric, $\beta_k(m)$ is a backward state metric and $\gamma_k(m)$ is a branch metric. These metrics can be rewritten as this:

$$\alpha_k(m) = \sum_{m'=0}^{M-1} \Pr(S_k = m, R_k | S_{k-1} = m', R_1^{k-1}) \Pr(S_{k-1} = m', R_1^{k-1})$$

$$= \sum_{m'=0}^{M-1} \Pr(S_{k-1} = m, R_1^{k-1}) \Pr(S_k = m, R_k | S_{k-1} = m') = \sum_{m'=0}^{M-1} \alpha_{k-1}(m').\gamma_k(m', m) \quad (3\text{-}5)$$

$$\beta_k(m) = \sum_{m'=0}^{M-1} \Pr(S_{k+1} = m', R_{k+1}^N | S_k = m) = \sum_{m'=0}^{M-1} \frac{\Pr(S_{k+1} = m', R_{k+1}^N, S_k = m)}{\Pr(S_k = m)}$$

$$= \sum_{m'=0}^{M-1} \Pr(S_{k+1} = m', R_{k+1} | S_k = m) \Pr(R_{k+2}^N | S_{k+1} = m') = \sum_{m'=0}^{M-1} \beta_{k-1}(m').\gamma_k(m, m') \quad (3\text{-}6)$$

Figure 3.5 shows how the above three metrics work in trellis codes. These are essential to compute $\lambda_k^i(m)$ which can be used to get $L(d_k)$.

Thus, $L(d_k)$ can be written using metrics

$$L(d_k) = \log \frac{P_r(d_k = 1 | R_1^N)}{P_r(d_k = 0 | R_1^N)} = \log \frac{\sum_m \lambda_k^1(m)}{\sum_m \lambda_k^0(m)} = \log \frac{\sum_m \sum_{m'} \alpha_{k-1}(m').\gamma_k^1(m, m').\beta_k(m)}{\sum_m \sum_{m'} \alpha_{k-1}(m').\gamma_k^0(m, m').\beta_k(m)} \quad (3\text{-}7)$$

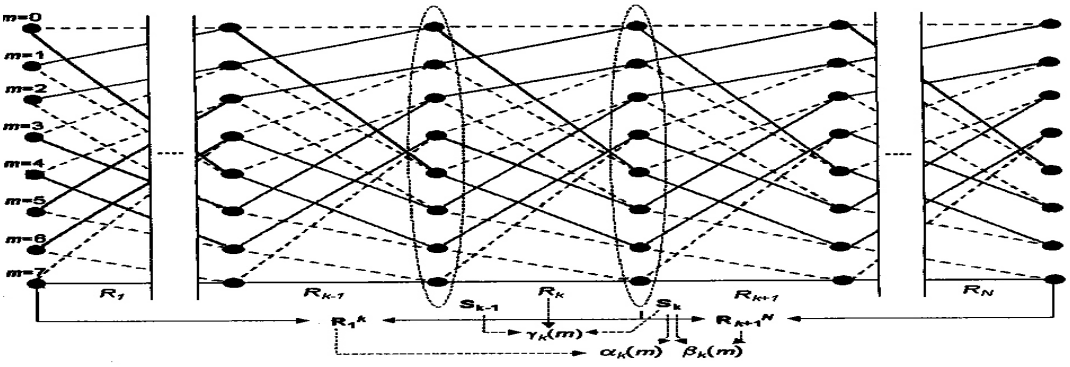

Figure 3.5 State and branch metrics dependencies in the MAP algorithm.
(Adopted from Ref. [16])

In the case of RSC encoders, the received values R_k are split into two uncorrelated components y_k^s and y_k^p, where y_k^s is the received systematic component and y_k^p is the coded parity component. Thus, log-likelihood can be rewritten as

$$L(d_k) = \log \frac{P_r(y_k^s \mid d_k = 1)}{P_r(y_k^s \mid d_k = 0)} \frac{\sum_m \sum_{m'} \alpha_{k-1}(m').\gamma_k^1(y_k^p, m, m').\beta_k(m)}{\sum_m \sum_{m'} \alpha_{k-1}(m').\gamma_k^0(y_k^p, m, m').\beta_k(m)}$$

$$= \log \frac{P_r(y_k \mid d_k = 1)}{P_r(y_k \mid d_k = 0)} + \log \frac{\sum_m \sum_{m'} \alpha_{k-1}(m').\gamma_k^1(m, m').\beta_k(m)}{\sum_m \sum_{m'} \alpha_{k-1}(m').\gamma_k^0(m, m').\beta_k(m)} \qquad (3\text{-}8)$$

The right side of the equation of (3-8) is extrinsic information.

3.3.2 Principles of Iterative Decoding

The second term in the right side of the equation of (3-8) is the redundant information which called extrinsic information. This information improves the LLR for bit d_k

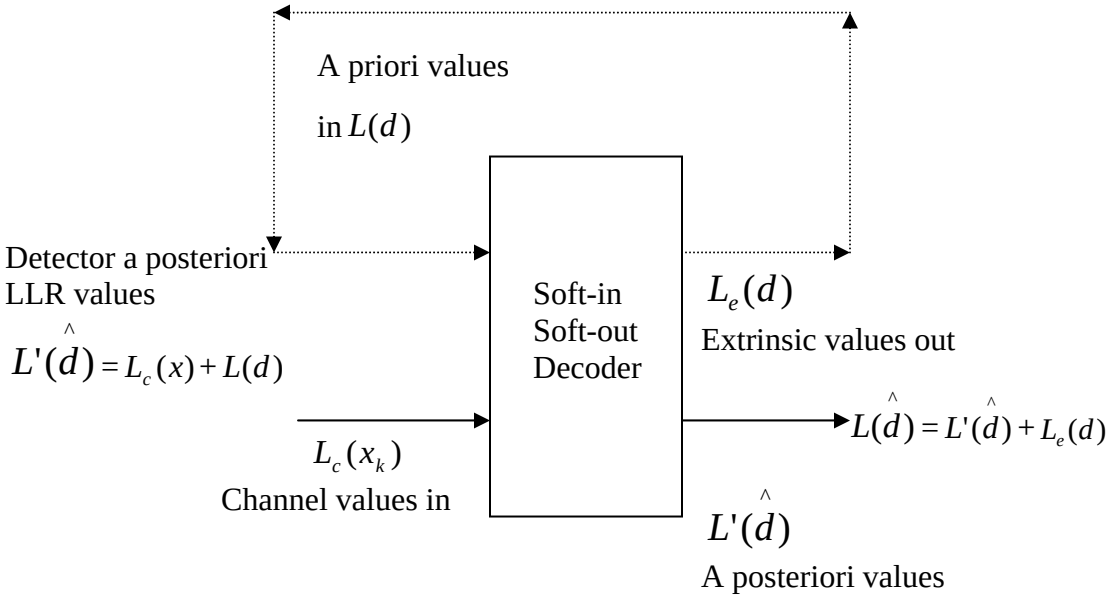

Figure 3.6 Soft-input soft-output decoder module.

Log-likelihood Ratio of the information bit conditioned by the received symbol is

$L(d_k \mid x_k) = \log \frac{P_r(d_k = 1 \mid x_k)}{P_r(d_k = -1 \mid x_k)}$. Using Bayes' rule, it can be changed like this:

$$L(d_k \mid x_k) = \log \frac{P_r(x_k \mid d_k = 1)}{P_r(x_k \mid d_k = -1)} + \log \frac{P_r(d_k = 1)}{P_r(d_k = -1)} \tag{3-9}$$

If AWGN channels are considered, the conditional pdf can be written as

$$p(x_k \mid d_k = 1) = \frac{1}{\sqrt{2\pi\sigma}} \exp(-\frac{1}{2\sigma^2}(x-1)^2), \; p(x_k \mid d_k = -1) = \frac{1}{\sqrt{2\pi\sigma}} \exp(-\frac{1}{2\sigma^2}(x+1)^2)$$

We can now compute

$$\log \frac{P_r(x_k \mid d_k = 1)}{P_r(x_k \mid d_k = -1)} = -\frac{1}{2}\left(\frac{(x_k - 1)^2}{\sigma}\right) + \frac{1}{2}\left(\frac{(x_k + 1)^2}{\sigma}\right) = -\frac{2}{\sigma^2} x_k = 4\frac{E_S}{N_0} x_k$$

Thus, we obtain

$$L(d_k \mid x_k) = 4\frac{E_S}{N_0} x_k + \log \frac{P_r(d_k = 1)}{P_r(d_k = -1)} = L_c(x_k) + L_a(d_k) \tag{3-10}$$

where $L_c(x_k) = 4\frac{E_S}{N_0} x_k$, $L_a(d_k) = \log \frac{P_r(d_k = 1)}{P_r(d_k = -1)}$: a priori value for bit d_k

If we consider the Log-likelihood Ratio of the information bit conditioned by the whole observation sequence, we can now rewrite

$$L(d_k) = L(d_k \mid x_k) + L_e(d_k) = L_c(x_k) + L_a(d_k) + L_e(d_k) \tag{3-11}$$

where $L_e(d_k)$ is the extrinsic information derived from equation of (3-7).

Decoder 1 sends the new reliablilty information to *Decoder 2*, and *Decoder 2* revises the first information by new information which came from *Decoder 1*. The two decoders alternately update their probability measures by iterations.

3.4 Simulation Results

The BER of the turbo coded system is presented in Figure 3.7. Matlab is used to make simulations. Generating polynomials are $(37,21)_{octal}$, which is the same Turbo codes used in the original paper [13], but 2000 of the number of information bits N are used which is different to the original paper.

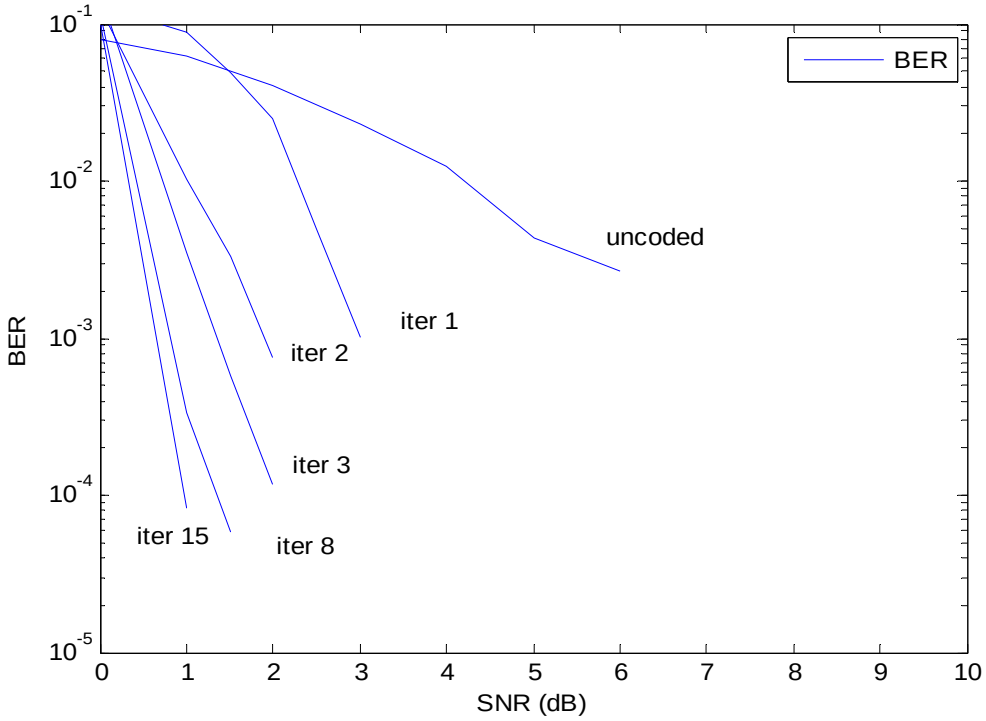

Figure 3.7 The BER performance of the Turbo over AWGN (N = 1000, Rate = $\frac{1}{2}$).

Figure 3. 7 shows that Turbo codes outperforms over the uncoded scheme. The result for 15 iterations is close to the 1 dB of SNR. It is remarkably improved and close to the Shannon limit. We also observe that as iterations are increased, the performance of the Turbo codes is improved. However, the gain is smaller as the iteration is larger.

Chapter 4 Low-Density Parity Check (LDPC) Codes

Low-Density Parity Check (LDPC) codes is a linear block code which is well known to correct errors in digital communication channels. LDPC codes was invented by Robert Gallager in the early 1960s [22]. However, it had been ignored for a long time due to the requirements of high complexity computations until it was rediscovered by Mackay in 1999 [23]. It has shown that LDPC codes is the best error correction code to close Shannon limit, which is the limitation in communication channels. Figure 4.1 shows the block diagram of LDPC codes. The mechanism of LDPC encoder is the same as the linear block encoder, but the main difference between LDPC codes and linear block codes are decoding algorithm. LDPC decoder uses sum-product algorithm which is a key technique for LDPC codes. Therefore, linear block code will be briefly described to understand LDPC encoder. Also, sum-product decoding algorithm will be discussed.

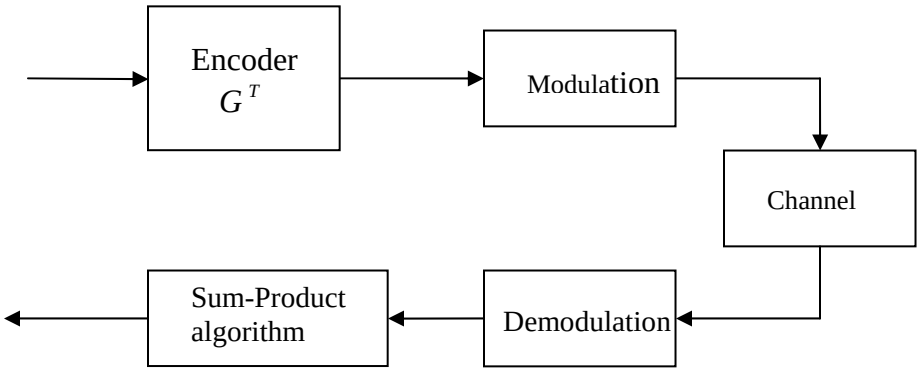

Figure 4.1 Block diagram of LDPC codes.

4.1 Fundamentals of Linear Block Codes

Generator matrix G is used to produce coded bits as depicted in Figure 4.2. Generator matrix G is related to parity check matrix H which is used at the receiver to find errors. Let $m_0, m_1, m_2, ...m_{k-1}$ constitute a block of k message bits and $b_0, b_1, b_2, ...b_{n-k-1}$ denote

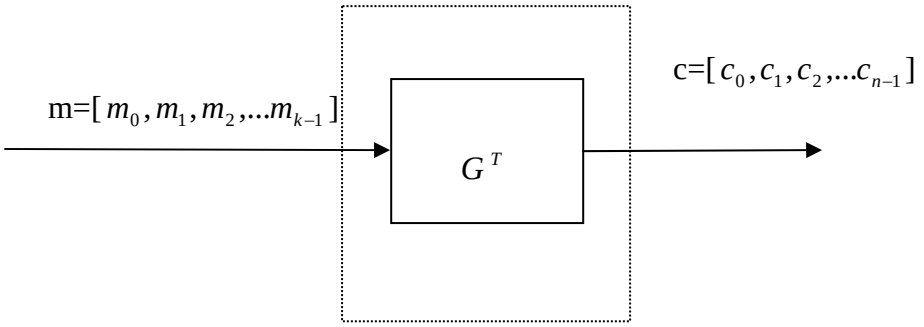

Figure 4.2 Block diagram of block code encoder.

the (n-k) parity bits in the code word and parity. Parity bits can be obtained by $b_{1\times(n-k)} = m_{1\times k} P_{k\times(n-k)}$ where P are one's if b depends on m, otherwise P are zero's. We may therefore write codeword c as follow:

$$c = [\, b : m] = m[\, P_{k\times(n-k)} : I_k\,] = mG \qquad (4\text{-}1)$$

where I_k is the *k* by *k* identity matrix and G is the generator matrix.

Let parity check matrix H = [$I_{n-k} : P_{(n-k)\times k}$], based on the eqation of (4-1) and parity check matrix H, $HG^T = 0$ can be obtained. Using this result, we can calculate cH^T to find errors which is called syndrome. For binary symmetric channel (BSC), the received codeword is *c* added with an error vector *e*. If we have the equation of $cH^T = 0$, all errors are detected.

4.2 LDPC Encoder

4.2.1 Parity Check Matrix H

In order to make LDPC codes, first, we need to make parity check matrix H. And then, generator matrix G can be made by parity check matrix H. Let us denote that M is number of row, N is number of column. H is represented as M×N matrix.

Parity check matrix H of LDPC codes is different from H of linear block codes. One

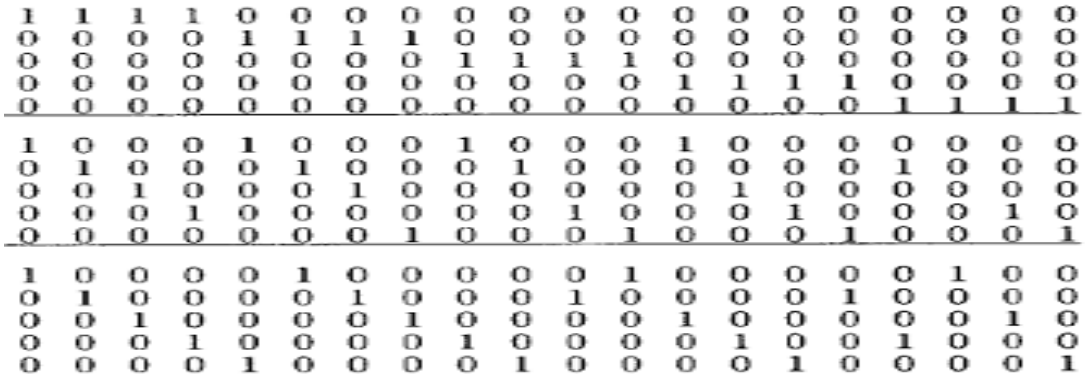

Figure 4.3 Parity check matrix (Adopted from Ref. [31])

remarkable characteristic of LDPC codes is that LDPC codes uses parity check matrix H which does not have identity matrix and contains very few 1's in each row and column. Define an (*N, j, k*) parity check matrix that has *j* ones in each column, and *k* ones in each row, and zeros elsewhere. Figure 4.3 shows a method to make H (20, 3, 4) which was introduced by Gallager [22]. Parity check matrix H is sub-divided into smaller sub-matrices (blocks) to ensure 1's are well dispersed. The first block of Figure 4.3 creates a single 1 in each column and the other blocks are merely a column permutated version of the first block. This is Gallager's method to make H, but there are many ways to make parity check matrix H [21][22][23].

If the number of 1's per column or row is constant, the code is called a regular LDPC codes, otherwise it is a irregular LDPC codes. Usually the irregular LDPC codes outperforms over other codes [21]. The key to make parity check matrix H is that the number of 1' in the matrix should be small.

4.2.2 Generator Matrix G

Given H, we can get generator matrix G to make encoder. Let H = [Z : X], where Z is a non singular matrix, H should be satisfied with $cH^T = 0$. Using this eqaution, parity bit b

can be rewritten $b = m(A^{-1}B)^T = mP$. And generator matrix G is

$$G = [\,(Z^{-1}X)^T \vdots I_K\,] \qquad (4-2)$$

Therefore, LDPC encoder can be made by generator matrix G.

4.3 LDPC Decoder

LDPC decoding algorithm has several names such as belief propagation algorithm, the message passing algorithm, and the sum-product algorithm. In this thesis, the name of sum-product algorithm will be used. Tanner graph [29] will be introduced first in order to explain sum-product algorithm,. And sum-product algorithm will be extended to work with soft decision.

4.3.1 Tanner Graph

Tanner graph is a bipartite graph which is an undirected graph whose nodes are divided into two classes, where edges only connect two nodes [30]. To understand Tanner graph,

Let us introduce a parity check matrix H

$$H = \begin{bmatrix} 1 & 0 & 1 & 0 & 1 & 0 & 1 \\ 0 & 1 & 1 & 0 & 0 & 1 & 1 \\ 0 & 0 & 0 & 1 & 1 & 1 & 1 \end{bmatrix} \qquad (4-3)$$

The parity check matrix H of (4-3) has 7 rows and 3 columns, and it can be represented by Tanner graph which is shown in Figure 4.4. The nodes of the tanner graph are separated into two distinctive sets and edges are only connecting nodes of two different types. The two types of nodes in a Tanner graph are called bit nodes and check nodes. Edges between bit nodes and check nodes indicate the participation of bit (variable) m in parity check n.

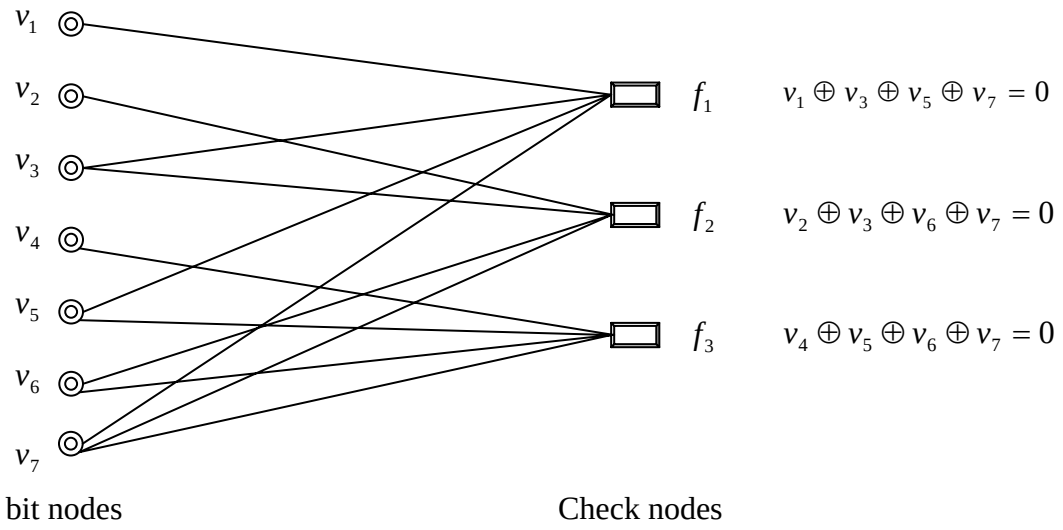

Figure 4.4 Tanner graph.

Tanner graph consists of m check nodes (the number of parity bits) and n variable nodes (the number of bits in a codeword). Check node c is connected to bit nodes b, provided that the element of H is one. As Tanner graph represents parity check matrix H, we can make decoder as simple as we can. For example, v_1 which is shown at the right side of Figure 4.4 should be the same with sum of modulo-2 of v_3, v_5 and v_7. It means that we can calculate v_1 using sum of modulo-2 of v_3, v_5 and v_7. Likewise, sum of modulo-2 of v_3, v_5 and v_7 can be used to get v_2. Each bit node updates their values using the probability of other bit nodes. The decoding is accomplished by iterating these steps. Tanner graph enables us to observe the algorithm as a good graphical view point. Now we are ready to look at the sum-product algorithm mathematically.

4.3.2 Soft Decision

At the receiver, the received bits are decoded 0 or 1. If the majority is 1, decoder chooses ‘1’, otherwise ‘0’ is chosen. It is called hard decision. Soft decision which is

based on the probability yields in a better decoding performance and it is concerned as the preferred method. Thus, the sum-product algorithm calculates approximations for log-likelihood ratios. The brief explanation for sum-product algorithm is like this.

Messages of probabilities of '1' or '0' are transmitted. Based on these probabilities, probabilities of bit nodes and probabilities of check nodes are updated. This procedure can be divided into three steps. First step is that bit nodes receive a message. In this step, a bit node has only a posteriori probability $p(x|y)$.

Second step is that bit nodes send a message to their check nodes which are connected each other. Check nodes send message back to the bit nodes after comparing incoming bits. For example, Tanner graph in Figure 4.4 shows that check node f_1 receives 4 bits from bits nodes. If the received bits are [1 0 0 1 0 1 0], check node f_1 sends [0 1 1 1] back to the bit nodes according to $v_1 \oplus v_3 \oplus v_5 \oplus v_7 = 0$.

Third step is to use additional information which came from check node. If the number of iteration is larger, bit nodes get more information from check nodes. Figure 4.5 depicts how messages are processed in tanner graph.

Below are steps for soft decision whose idea is the same as the above explanation. Input of the LDPC decoder is a posterior probabilities $p_n = p(c_n = x|y_n)$

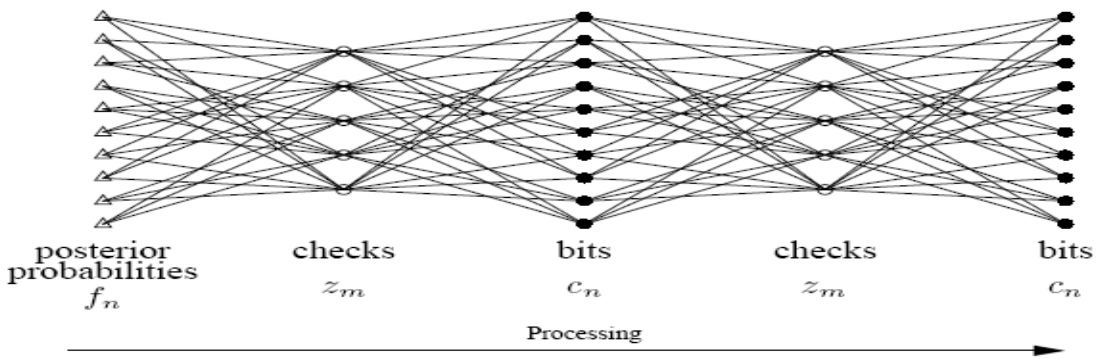

Figure 4.5 Factor graph at the LDPC decoder.

· **The first step** : **Initialization**

No other information other than a posteriori probability p_n is given in this step. The probability of the first step is written as

$$q_{mn}^{o} = p(x=0|y) \text{ and } q_{mn}^{1} = p(x=1|y) \quad (4\text{-}4)$$

· **The second step** : **Check node update**

Now we have a posteriori probabilities q_{mn}. The probabilities are sent to the check nodes. Check nodes calculate r_{mn} which is the conditional probability of check z_m being satisfied given by a bit c_n. Thus, r_{mn} is represented as $r_{mn} = P(z_m | c_n = x)$.

Let $\delta_{q_{mn}} = q_{mn}^{o} - q_{mn}^{1}$, and $\delta_{r_{mn}}$ be the product of $\delta_{q_{ij}}$ matrix elements along with row, excluding the (m , n) position. $\delta_{r_{mn}}$ can be written as $\delta_{r_{ij}} = \prod_{\{n' \in N_{m,n}\}} \delta_{q_{mn'}}$, where we define the set of bits that participate in check *m*, except for bit *n* is $\{N_{m,n} = N_m \setminus n\}$. The conditional probability of r_{mn} can be written as

$$r_{mn}^{0} = (1+\delta_{r_{mn}})/2 \text{ and } r_{mn}^{1} = (1-\delta_{r_{mn}})/2 \quad (4\text{-}5)$$

bit nodes Check nodes bit nodes Check nodes

(a) (b)

Figure 4.6 The illustration of (a) update check nodes (b) update bit nodes.

Figure 4.6 shows the illustration of updating check nodes and bit nodes.

· **The third step** : **Bit node update**

Now we have other information to update the values of the probability of q_{mn}^{o} and q_{mn}^{1}.

$$q_{mn}^{o} = \alpha_{mn} p_n^0 \prod_{\{m' \in M_{n,m}\}} r_{m'n}^0 \quad \text{and} \quad q_{mn}^{1} = \alpha_{mn} p_n^1 \prod_{\{m' \in M_{n,m}\}} r_{m'n}^1 \tag{4-6}$$

where constants α_n are selected to ensure $q_{mn}^1 + q_{mn}^0 = 1$. However, these probabilities are just used to do iterations. The pseudo posterior probability q_n is needed to get ultimate probabilities for bit nodes. If $q_n^1 > 0.5$, a decision is made that $x_n = 1$. q_n is written as

$$q_n = P(c_n = x | y_n, \{z_m = 0, m \in M_n\}) \tag{4-7}$$

The equation of (4-7) shows that all check nodes involving c_n are satisfied. It is also represented as

$$q_n^0 = \alpha_n p_n^0 \prod_{\{m' \in M_n\}} r_{m'n}^0 \quad \text{and} \quad q_n^1 = \alpha_n p_n^1 \prod_{\{m' \in M_n\}} r_{m'n}^1 \tag{4-8}$$

where constants α_n are selected to ensure $q_n^1 + q_n^0 = 1$.

Figure 4.7 shows the block diagram of LDPC decoder. Updating check nodes and bit nodes are iterated several times until all errors are detected.

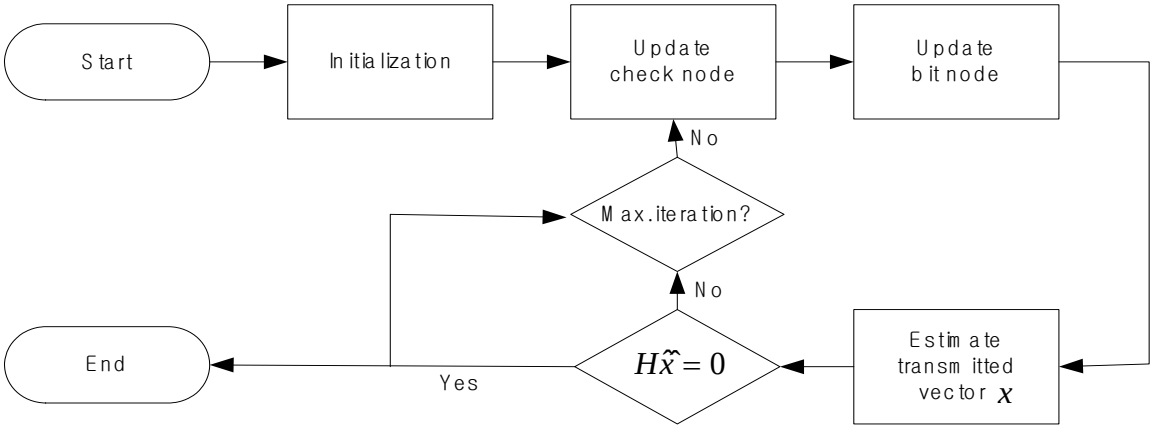

Figure 4.7 The block diagram of LDPC decoder.

4.4 Simulation Results

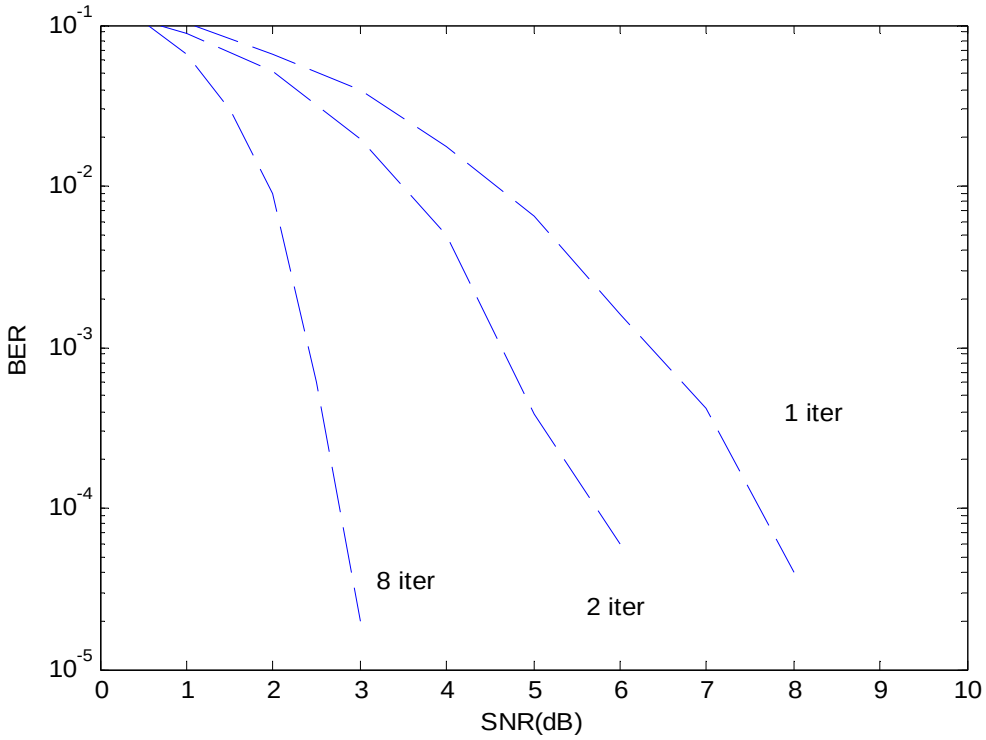

Figure 4.8 The BER performance of the LDPC over AWGN (N = 1000, Rate = $\frac{1}{2}$)

Figure 4.8 illustrates the BER of the LDPC coded system over AWGN channels. Regular parity check matrix is used that has 3 ones in each column, and 3 ones in each row. Sum-product algorithm is performed at the decoder with 8 iterations. And the numbers of bits, which are used in the simulation, are 1000.

Despite of small length of bits sequences, the graph shows that LDPC codes performs very well over AWGN channels. As the numbers of iterations were increased, we can see the fact that the result is closed to the zero.

Chapter 5 Design of Coded Modulation for Non-Coherent Fading Channels

In this Chapter, we will discuss the methods for coded modulations for non-coherent fading channels. Unitary space-time modulation, which is suitable for MIMO, is used to communicate over non-coherent fading channels. Since we have calculated capacity for single antenna and T of 2, we only consider one transmit and one receive antenna, and coherence time T will be restricted to 2. The results of this Chapter are shown in Chapter 6.

5.1 Turbo Codes with Unitary Space-Time Modulation

5.1.1 Encoding

Figure 5.1 illustrates how to combine turbo codes with unitary space-time modulation. Message bits are divided into blocks of N bits and are encoded by Turbo codes. As we discussed in Chapter 4, the turbo encoder consists of two recursive systematic convolutional encoders and it produces three types of outputs. Then, the encoded bits are interleaved by pseudorandom interleaver which is used to spread burst errors. However, the interleaver which is used at transmitter is different from the interleaver which is used in turbo encoder. And the next step is to modulate the interleaved data. Unitary space-

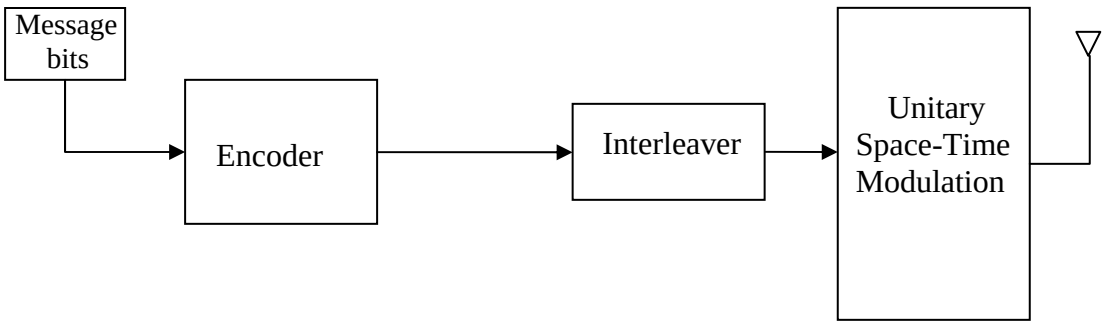

Figure 5.1 The block diagram of the channel encoder and unitary space-time modulation.

time modulation divides the interleaved bits into a constellation of L signals [10]. Given the coherence time of the channel of T, one transmit and one receive antenna, the transmitted signal matrix S from a unitary space-time constellation is like this

$$S_l = \sqrt{T}\Phi_l \qquad l = 1, \ldots, L, \tag{5-1}$$

where Φ_l is an isotropically distributed T×1 matrix and obeys $\Phi_l{}^{+}\Phi_l = I$.

The channel gain is constant for a period of T symbols when the unitary space-time modulation is used over a Rayleigh flat-fading channel.

5.1.2 Decoding

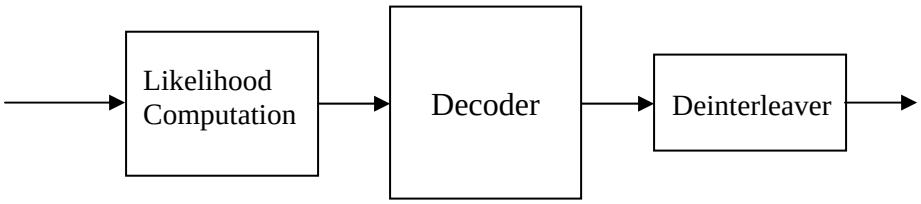

Figure 5.2 The block diagram of the receiver with channel decoder.

Hochwald and Marzetta's paper [10] shows maximum-likelihood (ML) algorithm and its performance when H is unknown. In their paper, maximum-likelihood decoding becomes

$$\Phi_l = \arg \max_{\Phi_l \in \{\Phi_1, \cdots, \Phi_L\}} \operatorname{tr}\left\{X^{+}\Phi_l \Phi_l^{+} X\right\} \tag{5-2}$$

However, instead of using the equation of (5-2), we will use a suboptimal decoding algorithm which computes the log-likelihoods of the transmitted bits, and uses them as if they are the log-likelihoods of the observations from a BPSK modulation over an AWGN [14][15][16]. This approach enables turbo codes to calculate the received data easily. It is also used in LDPC codes.

Notice that the received signal X corresponds to TR coded bits, where R is bit rate. We should compute the log-likelihoods of TR coded bits using received set of signals. Let us denote the TR bits $b = (b_1, \cdots, b_T, \cdots b_{TR})$ that construct S, then LLR can be written as

$$\Lambda(b_l) = \log \frac{\Pr\left[b_l = 1 \middle| X_1, \cdots, X_m\right]}{\Pr\left[b_l = 0 \middle| X_1, \cdots, X_m\right]} = \log \frac{\Pr\left[b_l = 1, X_1, \cdots, X_m\right]}{\Pr\left[b_l = 0, X_1, \cdots, X_m\right]}$$

$$= \log \frac{\sum_{b:b_l=1} \Pr\left[b_l = 1, X_1, \cdots, X_m\right]}{\sum_{b:b_l=0} \Pr\left[b_l = 0, X_1, \cdots, X_m\right]} \tag{5-3}$$

Assuming f ( ) is the mapping from *b* to *C* and that constellation. Signals are equiprobable, equation of (5-3) can be written as

$$\Lambda(b_l) = \log \frac{\sum_{S:S=f(b),b_l=1} \Pr\left[X \middle| S\right]}{\sum_{S:S=f(b),b_l=0} \Pr\left[X \middle| S\right]} \tag{5-4}$$

This equation explains how we use the LLR as if they are the LLR of the observations from a BPSK modulation over an AWGN channel. In Chapter 2, the equation of (2-3) is the conditional probability density of the received signals given the transmitted signal. Thus, we can rewrite the LLR of (5-4) as

$$\mathrm{LLR}(d_k) = \frac{\sum_{\Phi=S/\sqrt{T}:S=f(d),d_l=1} \exp(tr\left\{\frac{1}{1+1/T\rho} X^+ \Phi\Phi^+ X\right\})}{\sum_{\Phi=S/\sqrt{T}:S=f(d),d_l=0} \exp(tr\left\{\frac{1}{1+1/T\rho} X^+ \Phi\Phi^+ X\right\})} \tag{5-5}$$

Now, we have LLR for non-coherent fading channels. The LLR is considered as LLR of BPSK over AWGN channel. Therefore, the received bits are computed using (5-5) and are fed to turbo decoder. The turbo decoder iterates several times until it gets good results

and makes a decision whether received bits are zero or one. Then the decoded data are deinterleaved as the same order of interleaver to get original information bits.

5.2 LDPC Codes with Unitary Space-Time Modulation

5.2.1 Encoding

The basic concept of LDPC encoder with unitary space-time modulation is the same as the turbo encoder. Information bits are encoded by LDPC encoder and then interleaved by pseudo-random interleaver. Unitary space-time modulation modulates the interleaved bits using relevant codeword which will be introduced in Chapter 5.3. We consider only coherence time of 2. Thus, if a constellation of unitary space-time signals with L = 2 is used at the transmitter, code rate for modulation will be ½.

Generator matrix G, which is obtained by parity check matrix H, is needed to encode the information bits. Regular parity check matrix H in which the number of 1's in each row and column are the same will be used. In this thesis, Radford M. Neal' parity check matrix will be followed [18]. We will construct matrix which has all '0' element according to code rate and size of information bits. And then, we will exchange '0' for '1' randomly. After that, generator matrix G can be made by parity check matrix H.

5.2.2 Decoding

Figure 5-3 is the decoding algorithm for LDPC for non-coherent fading channels. Suboptimal decoding algorithm, which is used in turbo decoding, will compute the log-likelihood ratio. The outputs of LLR are fed into the LDPC decoder. LDPC decoder, which uses sum-product algorithm, considers the inputs as if they are the log-likelihoods of the observations from a BPSK modulation over an AWGN channels. So, the sum-product algorithm, which Chapter 4 introduced, performs at the decoder by updating

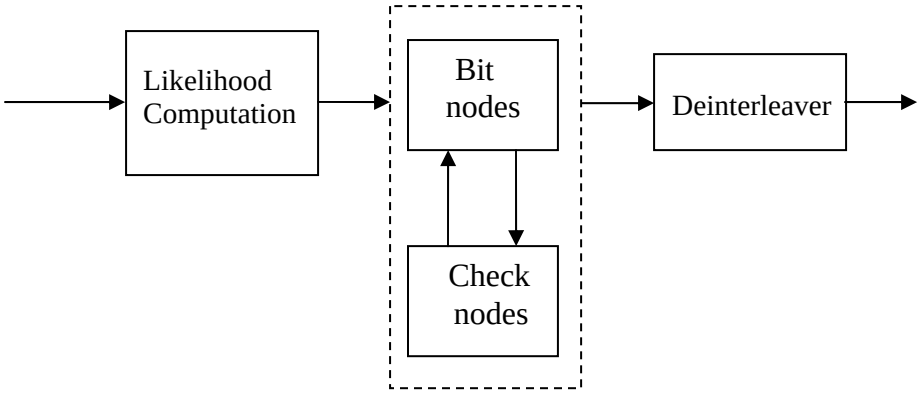

Figure 5.3 The block diagram of the receiver with LDPC decoder.

check nodes and bit nodes. Since information bits are interleaved at the transmitter, deinterleaver is needed at the receiver to reorder the output bits of the decoder.

5.3 Codewords

We list the code design that will be used in Chapter 6. These are known as optimum codewords for unitary space-time modulation, when coherence time T is 2. Turbo codes and LDPC codes will use these codewords for non-coherent channel to get the best results. These are provided by Professor Xue-Bin Liang.

When L = 2, the codeword is constructed as

1 0

0 1

When L = 4, the codeword is given as

0.17190316188463 + 0.01322163535223i 0.67654214840246 + 0.71593659825970i

-0.54002676136650 + 0.65232364799100i -0.05616595573097 + 0.52885758073090i

-0.29810582814894 + 0.63974297625038i 0.61238591922830 - 0.35615351394146i

-0.31464849171711 + 0.80992444881883i -0.41323442221031 - 0.27249958929542i

When L = 8, the codeword is constructed as

0.29969271052181 + 0.02912970218342i -0.89689754263130 - 0.32389896222854i

0.43688459027774 - 0.89034326540829i	-0.10202752854343 - 0.07753133520894i
0.61276223332760 - 0.05732985392968i	-0.20959209439429 + 0.75980713817599i
-0.73620835244785 + 0.07063610459637i	-0.53973844829382 + 0.40210721200552i
0.36138307080957 + 0.62268397318539i	0.47931532464102 - 0.50192007853300i
0.81049080062371 - 0.06333528832554i	-0.57975652026951 + 0.05454979891852i
0.62690317031624 - 0.55536407934685i	0.54562564956055 + 0.02925414432706i
0.34307330546712 - 0.04030025461337i	0.87575116458335 + 0.33724841628222i

Chapter 6 Simulation Results

Based on Chapter 5, Turbo codes and LDPC codes will be applied for non-coherent channels. Coherence interval T = 2 will be considered in this thesis. Matlab is used to make all simulations in this Chapter. And several web pages are referred in order to make LDPC codes and Turbo codes [12][19][20].

6.1 Simulation Results of Turbo Codes

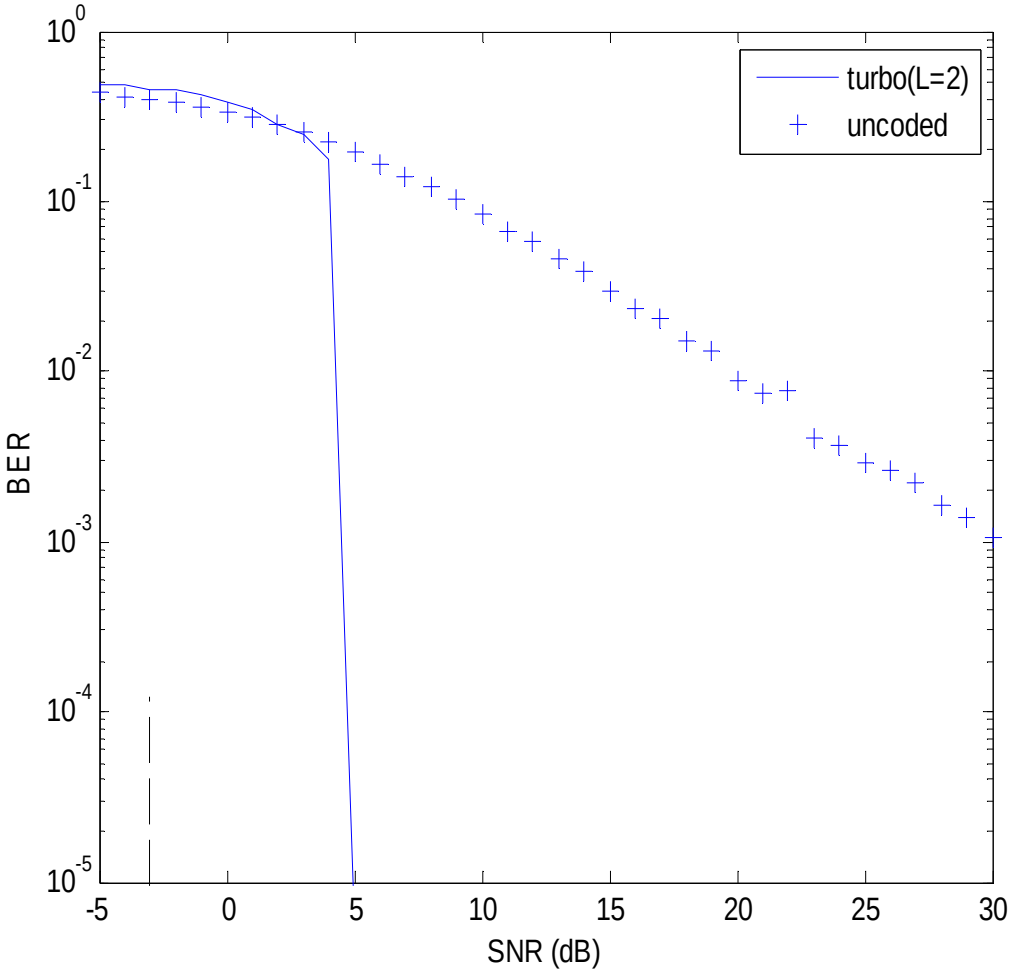

Figure 6.1 Turbo codes in non-coherent channel (T=2) for one transmit antenna and one receive antenna (L=2).

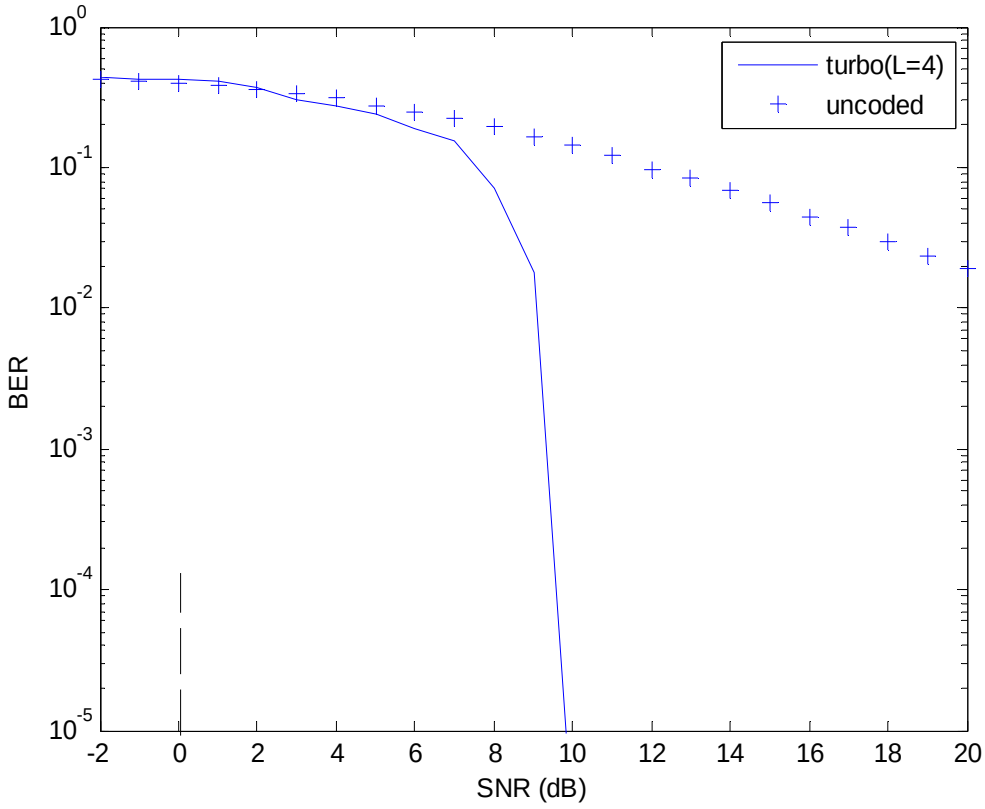

Figure 6.2 Turbo codes in non-coherent channel (T=2) for one transmit antenna and one receive antenna (L=4).

6.1.1 Performance Evaluation of Turbo-Coded Modulation Scheme

The above graphs illustrate simulations of Turbo codes in terms of bit error rate versus signal-to-noise ratio (SNR) for one transmit antenna and one receive antenna. $(g_n, g_d) = (37,21)_{octal}$ generating polynomials are used which is the same turbo codes used in the original turbo coding paper [13]. The numbers of information bits which are used in the simulation are 2000 and the rate of the turbo codes is $\frac{1}{2}$. Based on Chapter 2, capacity for non-coherent channels is depicted as a dashed line. Figures 6.1 and 6.2 demonstrate channel capacity, Turbo codes and uncoded modulation for non-coherent

fading channel. Clearly, simulation results demonstrate that the Turbo codes have good performance in non-coherent fading channels.

However, when comparing the results with the capacity, more than 5 dB between capacity and simulation result are found. The graph shows approximately 8 dB, when constellation L is 2. When constellation L is 4, we can find less than 10 dB. This gap is large compared to the performance over AWGN channels.

6.2 Simulation Results of LDPC Codes

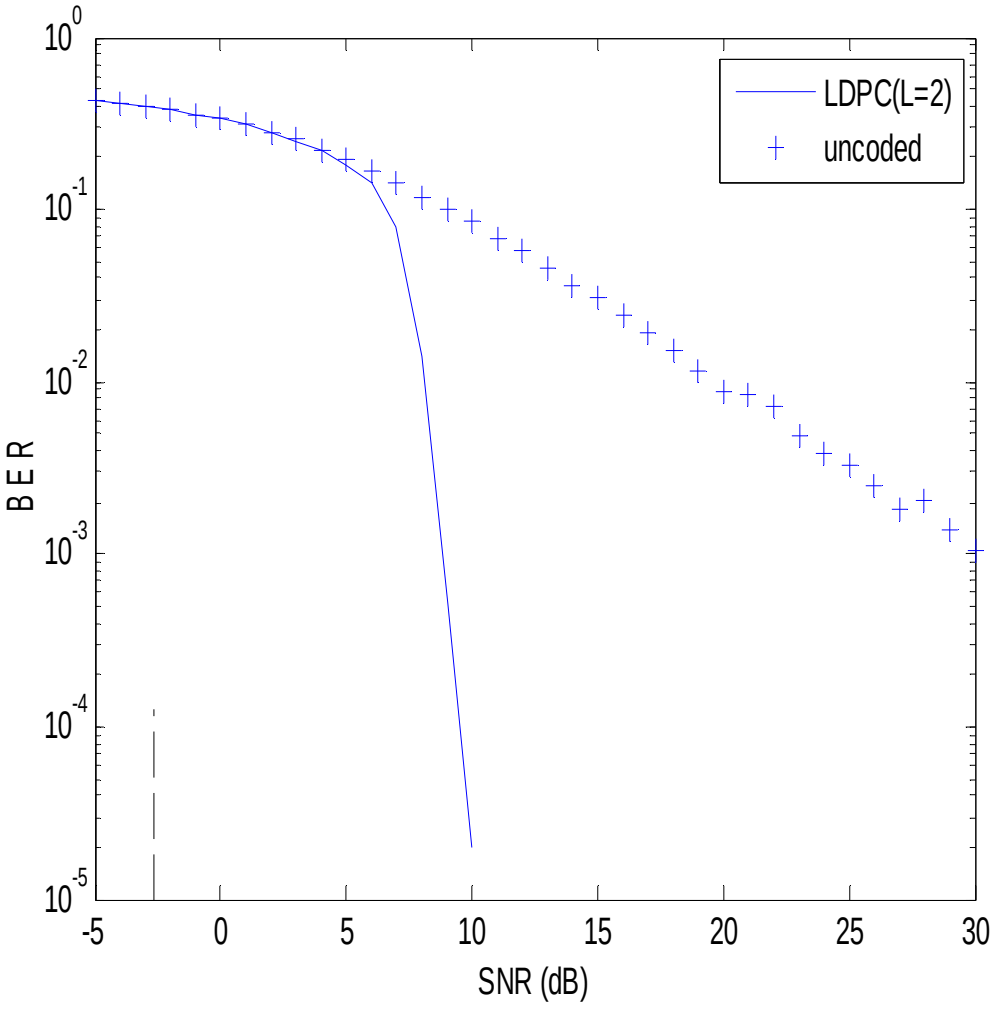

Figure 6. 3 LDPC codes in non-coherent channel (T=2) for one transmit antenna and one receive antenna (L=2).

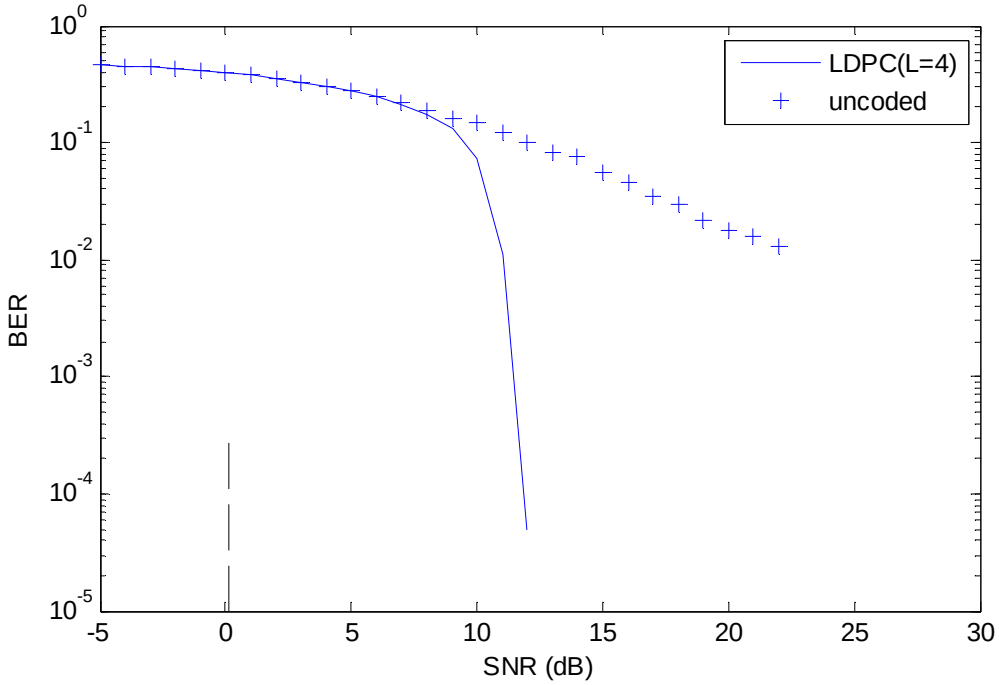

Figure 6. 4 LDPC codes in non-coherent channel (T=2) for one transmit antenna and one receive antenna (L=4).

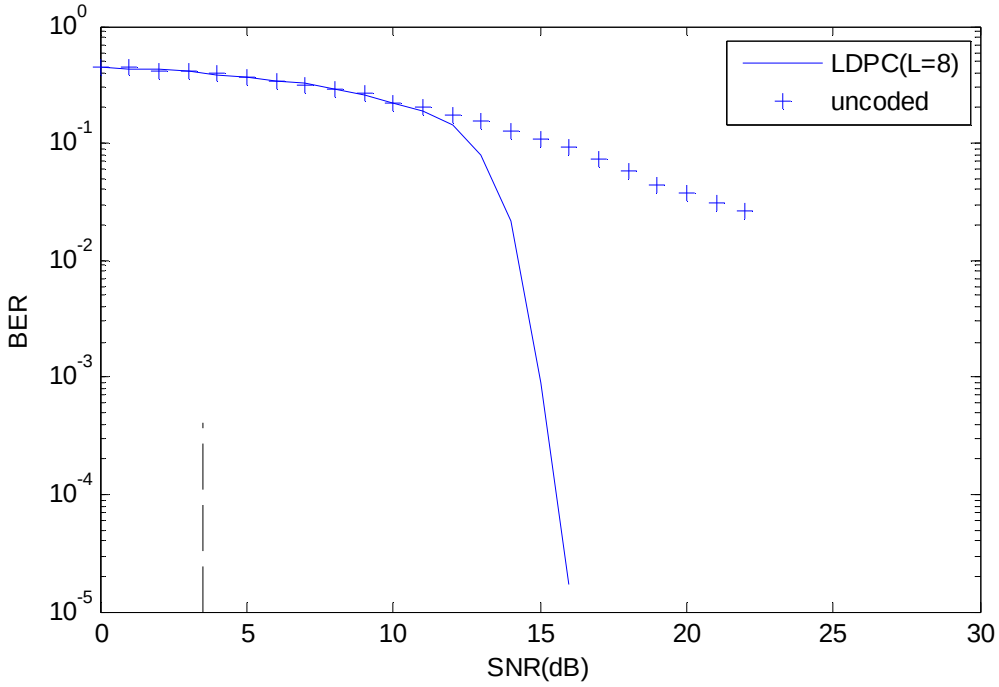

Figure 6. 5 LDPC codes in non-coherent channel (T=2) for one transmit antenna and one receive antenna (L=8).

6.2.1 Performance Evaluation of LDPC-Coded Modulation Scheme

Despite communication toolbox for matlab gives LDPC codes function, we follow several websites which have matlab based LDPC source codes to understand LDPC codes [19] [20]. The regular low density parity check matrix H, which is based on Radford M. Neal's programs collection [18], is used in this paper. The number of 1's in each row and column of $\frac{1}{2}$ parity check matrix H are 3. And parity check matrix H for our simulations makes only rates. At the receiver, soft decision is used which is better than hard decision for BER versus SNR performance. 8 iterations are executed to obtain better results.

Three graphs of Figure 6.3, 6.4, and 6.5 show LDPC codes performed over non-coherent fading channels for single antenna and coherence time T of 2. As can be expected, LDPC codes demonstrate the great results compared to uncoded non-coherent channel. LDPC codes for non-coherent channel is closer to the Shannon limit.

However, the results are not close to the capacity as we expected. It has approximately 12 dB gaps. Both Turbo codes and LDPC codes perform well in non-coherent fading channels, but they are not close to the capacity which we computed. We can assume that it is not sufficient to just combine channel coding with non-coherent channels. To reduce the gap, other factors may be considered or encoding and decoding algorithm should be modified.

Chapter 7 Conclusion

We have calculated channel capacity for non-coherent fading channels. Because of complexity, capacity for channels of coherence time T = 2 and single antenna is considered and computed. Based on this capacity, we have used LDPC codes and Turbo codes to approach the capacity.

Unitary space-time modulation has also been introduced. It performs well for Rayleigh fading environment, when the receiver does not know the channel state information. Optimum codewords for unitary space-time modulation have been used to get better performance. Also, unitary space-time modulation has been combined with channel coding.

The results have shown that coded unitary space-time modulation scheme has performed significantly better than the uncoded unitary space-time modulation alone, when the channel state information is not available for both transmitter and receiver.

Furthermore, iterations for channel coding perform well for non-coherent fading channels. However, when we compare the performance result to the capacity which we calculated in Chapter 2, it is not as good as that for AWGN channels, even though the

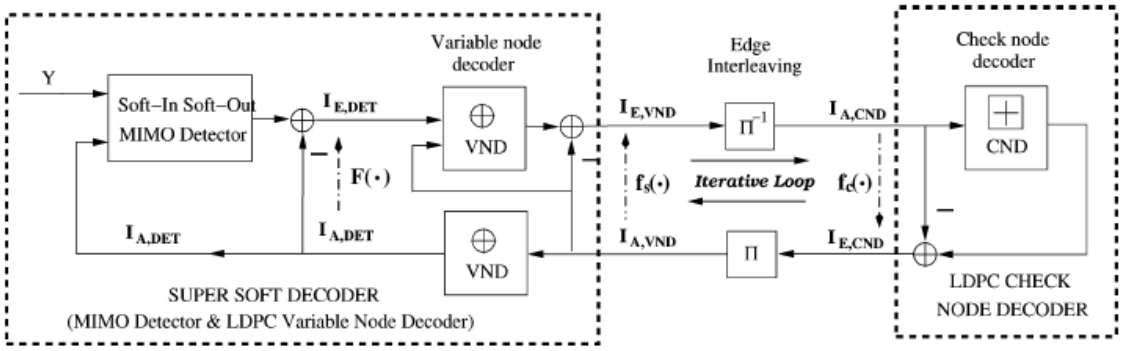

Figure 7.1 New receiver structure of LDPC-coded MIMO system (Adopted from Ref. [27])

best codewords for constellation are used. There exists more than 8dB gap between Shannon limit and the actual performance.

We can analyze some reasons why the gap exists. We have just combined channel coding with unitary space-time constellation without any modification. There are other papers which try to modify the decoding algorithm to get better performance [15][27], but these papers do not mention the channel capacity, so we do not know whether or not the results of the simulation are close to the channel capacity. Figure 7.1 shows a method of [27] for LDPC codes for non-coherent fading channels. Modifying the decoding algorithm may be one of the ways to reduce the gap.

Moreover, we have used small number of information bits and special coherence time T of length 2. Further research can be carried out for a large number of information bits to get better performance, because long channel coding has performed close to the Shannon limit [23]. Also, increasing coherence time T may improve the performance. They are still left open for further research.

Bibliography

[1] D. Tse and P. Viswanath, *Fundamentals of Wireless Communication*, Cambridge University Press, 2000.

[2] H. L. Bertoni, *Radio Propagation for Modern Wireless Systems*, Prentice Hall, 2000.

[3] J. G. Proakis, *Digital Communications, 4th ed.* New York: McGraw-Hill, 2001.

[4] A. Goldsmith, *Wireless Communications*, Cambridge University press, 2005.

[5] T. L. Marzetta and B. M. Hochwald, "Capacity of a mobile multiple-antenna communication in Rayleigh flat fading," *IEEE Trans. Inform. Theory*, vol. 45, pp.139–157, Jan. 1999.

[6] B. M. Hochwald, T. L. Marzetta, T. J. Richardson, W. Sweldens, and R. Urbanke, "Systemic design of unitary space-time constellations," *IEEE Trans. Inform. Theory*, vol. 46, pp. 1962–1973, Sept. 2000.

[7] B. Hassibi and T. L. Marzetta, "Multiple-antennas and isotropically random unitary inputs: The received signal density in closed form," *IEEE Trans. Inform. Theory*, vol. 48, pp. 1473–1484, Jun. 2002.

[8] C. E. Shannon, "A mathematical theory of communication," *Bell Syst. Tech. Journal*, vol. 27, 1948, pp. 379–423 and pp. 623–656.

[9] R. W. Hamming, "Error detecting and error correcting codes," *Bell Syst. Tech. Journal*, vol. 29, pp. 147–160, 1950.

[10] B. M. Hochwald and T. L. Marzetta, "Unitary space-time modulation for multiple-antenna communications in Rayleigh flat fading," *IEEE Trans. Inform. Theory*, vol. 46, pp. 2041–2052, Mar. 2000.

[11] D. Gesbert, D. Shiu, P. J. Smith, and A. Naguib, "From theory to practice: An overview of MIMO space-time coded wireless systems," *IEEE Journal. Select. Area Commun.*, vol. 21, no. 3, pp. 281–302, Apr. 2003.

[12] Y. Wu, http://www.ee.vt.edu/~yufei/turbo.html

[13] C. Berrou, A. Glavieux, and P. Thitimajshima, "Near Shannon limit error-correcting coding and decoding: Turbo-codes," in *Proc. IEEE Int. Conf. Commun. (ICC)*, 1993, pp. 1064–1070.

[14] A. Stefanov and T. M. Duman, "Turbo coded modulation for systems with transmit and receive antenna diversity," in *Proc. IEEE Global Commun. Conf. (Globecom)*, vol. 5, 1999, pp. 2336–2340.

[15] I. Bahceci and T. M. Duman, "Combined turbo coding and unitary space-time modulation," *IEEE Trans. Commun.*, vol. 50, pp. 1244–1249, Aug. 2002.

[16] A. Giulietti, B. Bougard, and L. V. der Perre, *Turbo Codes Desirable and Designable*, Boston : Kluwer Academic Publishers, 2004.

[17] A. Stefanov and T. M. Duman, "Turbo coded modulation for systems with transmit and receive antenna diversity over block fading channels: System model, decoding approaches and practical considerations," *IEEE Journal. Select. Areas Commun.*, vol. 19, pp. 958–968, May 2001.

[18] R. M. Neal, http://www.cs.toronto.edu/~radford/ftp/LDPC-2006-02-08/

[19] A. Avudainayagam, http://arun-10.tripod.com/ldpc/ldpc.htm

[20] B. S. Nugroho, http://bsnugroho.googlepages.com/ldpc

[21] T. J. Richardson, M. A. Shokrollahi, and R. L. Urbake, "Design of capacity-approaching irregular low-density parity-check codes," *IEEE Trans. Inform. Theory*, vol. 47, no. 2, pp. 619–637, Feb. 2001.

[22] R. G. Gallager, *Low-Density Parity-Check Codes,* Cambridge, MA: M.I.T. Press, 1963.

[23] D. J. C. MacKay and R. M. Neal, "Near Shannon limit performance of low density parity check codes," *IEE Electronics Letters*, vol. 32, no. 18, pp. 1645–1655, Aug. 1996.

[24] D. J. C. MacKay, "Good error-correcting codes based on very sparse matrices," *IEEE Trans. Inform. Theory*, vol. 45, pp. 399–431, Mar. 1999.

[25] W. E. Ryan, "An introduction to LDPC codes," preprint, Aug. 2003.

[26] B. M. J. Leiner, "LDPC codes- a brief tutorial," preprint, Apr. 2005.

[27] J. Zheng and B. D. Rao, "LDPC-coded MIMO systems with unknown block fading channels: soft MIMO detector design, channel estimation, and code optimization," *IEEE Trans. Signal Processing*, vol. 54, no. 4, pp. 1504–1518, Apr. 2006.

[28] S. Haykin, *Communication Systems, 4th ed*. House of Electronics Industry, 2003.

[29] F. R. Kschischang, B. J. Frey, and H. Loeliger, "Factor graphs and the sum-product algorithm," *IEEE Trans. Inform. Theory*. vol. 47, no. 2, pp. 498–519, Feb. 2001.

[30] J. Sun, “An introduction to low density parity check (LDPC) codes,” preprint, Jun. 2003.

[31] www.cs.wustl.edu/~jain/cse574-06/ftp/j_3phy/sld012.htm

[32] www.regenttechnology.com/Solutions/4G.htm

Vita

Youngjeon Cho was born in Chunnam, Korea, in September, 1976. After completing his high school education at Kwang-ju in February 1995, he enrolled at the Korea Military Academy to become an Army officer. After completing his bachelor of science degree in electrical engineering in March 1999, he has served as an Army officer in the Korea Army. The Korea army selected him into a government-funded program for advanced study abroad and he entered Louisiana State University in August 2006 to get his master's degree.

Currently, he is a candidate for the degree of Master of Science in Electrical Engineering at Louisiana State University, which will be awarded at the May 2008 commencement.